From the Institute for Bioinnovation

BSRC “Alexander Fleming”, Vari, Greece

Integrin-mediated adhesion in tumour vasculature

Maria A. Koufaki

M.Sc. MOLECULAR BIOMEDICINE: MECHANISMS OF DISEASE, MOLECULAR AND CELLULAR THERAPIES, AND BIOINNOVATION

HELLENIC REPUBLIC
National and Kapodistrian University of Athens

"ALEXANDER FLEMING"
Biomedical Sciences Research Center

Athens 2020

MASTER THESIS

Title of the Master thesis

Integrin-mediated adhesion in tumour vasculature

Submitted by

Maria A. Koufaki

In partial fulfilment of the requirements for the degree of **Master of Science (M.Sc.)** in **Molecular Biomedicine: Mechanisms of disease, molecular and cellular therapies, and bioinnovation**

Three-membered Examination Committee

Vassiliki Kostourou (Supervisor)

Institute for Bioinnovation

BSCR "Alexander Fleming", Vari, Greece

Antigone Dimas

Institute for Bioinnovation

BSRC "Alexander Fleming", Vari, Greece

Aristides G. Eliopoulos

Department of Biology, School of Medicine

National and Kapodistrian University of Athens, Athens, Greece

ABSTRACT

Beyond the conventional perception of solid tumours as mere masses of cancer cells, advanced cancer research focuses on the complex contributions of tumour-associated host cells that are known as "tumour microenvironment". Established regulators of cancer progression are the endothelial cells (ECs) comprising the angiogenic tumour vasculature. The integrin-related signalling has a profound influence on multiple aspects of tumour growth including vessel formation, yet the effects of altered expression of integrin mediators remain unclear. PINCH is considered as a crucial adaptor protein of integrin-dependent signalling. Two members of the PINCH protein family (PINCH1 and PINCH2) have been identified and are expressed in a variety of mammalian tissues. Here, we aim to address the impact of PINCH1 on tumour-associated neovasculature. In particular, we applied a comprehensive approach to investigate the lack of PINCH1 expression on murine endothelium in syngeneic tumour models (lung adenocarcinoma or melanoma-induced subcutaneous tumours). EC-specific PINCH1 ablation led to decreased growth of lung adenocarcinoma but not melanoma tumours. Attenuated tumour progression was accompanied by decreased vessel leakage in knockout (KO) tumours compared to control. To address potential biological compensation, we confirmed PINCH2 expression by ECs and generated double PINCH KO tumour-bearing mice. Complete PINCH ablation from ECs resulted in reduced volume and is likely to affect the vessel density of lung adenocarcinoma-derived tumours. Together, our work offers valuable insight into the role of PINCH1 and PINCH2 on cancer biology using *in vivo* tumour model approaches and imaging technology.

Based on recent findings in the lab, the second aim of this study was to explore the presence of local RNA translation on integrin-related structures (termed as focal adhesions or FAs) of ECs. After extensive protocol modifications and standardization, we managed to isolate sufficient amounts of high-quality RNA from EC FAs, supporting the FA-localized translation hypothesis.

Keywords: Integrin signalling, tumour angiogenesis, endothelial cells, PINCH, focal adhesions, RNA translation

ACKNOWLEDGMENTS

I greatly acknowledge **Dr Vassiliki Kostourou** for helpful and devoted supervision throughout my thesis, available at all times.

This thesis would not be completed without the extensive experimental guidance, cooperation and, above all else, great company of current and past members of Dr Kostourou laboratory, **Christina Arapatzi**, **Pinelopi Nikolopoulou**, **Georgia Rouni**, **Eva Giannaki**, **Dr Vassiliki Papadaki** and **Christos Kamaras**.

I would like to thank **Dr Antigone Dimas** for her generous and valuable advice regarding both personal and scientific matters.

I also thank **Dr Vaggelis Harokopos**, **Dr Sofia Grammenoudi**, **Dr Vasileios Ntafis** and corresponding scientific staff for technical assistance at the genomics facility, flow cytometry facility and animal house of BSRC "Alexander Fleming", respectively.

I am also grateful to **Lilian Voudouri foundation** for important financial support during my MSc studies.

Last but not least, I own many thanks and appreciation to my **family** for embracing my worries and endorsing my decisions.

TABLE OF CONTENTS

LIST OF ABBREVIATIONS

ANG-2	Angiopoietin-2
ANK	Ankyrin
BMDCs	Bone-marrow-derived cells
BSA	Bovine serum albumin
C-terminus	Carboxy-terminus
CAFs	Cancer-associated fibroblasts
CH	Calponin homology
CSCs	Cancer stem cells
DABCO	1, 4-Diazabicyclo-octane
DAPI	4′,6-diamidino-2-phenylindole
DMEM	Dulbecco's modified Eagle's medium
dNTPs	Deoxy-nucleotide triphosphates
DPBS	Dulbecco's PBS
E	Embryonic day
ECM	Extracellular matrix
ECs	Endothelial cells
EGF	Epidermal growth factor
EPCs	Endothelial precursor cells
ES cells	Embryonic stem cells
HSCs	Haematopoietic stem cells
HUVECs	Human umbilical vein endothelial cells
FAK	Focal adhesion kinase
FAs	Focal adhesions
FBS	Fetal bovine serum
IAC	Integrin-associated complex
ICAP-1	Integrin cytoplasmic domain- associated protein 1
ILK	Integrin-linked kinase
IMLECs	Immortalized mouse lung endothelial cells
IPP	ILK-PINCH-parvin
IV	Intravenous
KO	Knockout
LIM	LIN-11, Isl1 and MEC-3
LLC	Lewis lung carcinoma
MLECs	Mouse lung endothelial cells

MMPs	Matrix metalloproteinases
PBS	Phosphate-buffered saline
PCR	Polymerase chain reaction
PECAM-1/PECAM (CD31)	Platelet-endothelial cell adhesion molecule-1
PFA	Paraformaldehyde
PH	Pleckstrin homology
PIGF	Placental growth factor
PINCH	Particularly interesting new cysteine-histidine-rich protein
PK	Proteinase K
PDGF-β	Platelet-derived growth factor-β
RBPs	RNA binding proteins
RSU-1	Ras suppressor-1
SHANK	SH3 and multiple ankyrin repeat domains protein
SCs	Stalk cells
TAE	Tris acetate EDTA
TAM	Tamoxifen
TCs	Tip cells
TECs	Tumour-associated endothelial cells
TGF-β	Transforming growth factor-β
VE-cadherin (CD144)	Vascular endothelial cadherin
VEGF	Vascular endothelial growth factor
VEGFR	Vascular endothelial growth factor receptor
VPF	Vascular permeability factor
vSMCs	Vascular smooth muscle cells
WFI	Water for injection

1. INTRODUCTION

As stated by the World Health Organization (www.who.int/), cancer is the second-ranked disease with the highest mortality rates worldwide, accounting for approximately 9.6 million lives (one to six people died from cancer rather than any other cause) in 2018. Malignant cells are the main driving force of tumour formation and growth, yet they do not manifest the disease single-handed. It is now increasingly accepted that non-cancerous cells present in the tumour contribute to the hallmark capabilities[1] and enabling characteristics[2] of cancer as aptly described by D. Hanahan and R. A. Weinberg (**Fig. 1A and 1B**). Tumour-associated host cells include cancer-associated fibroblasts (CAFs), infiltrating immune cells of both myeloid (for instance macrophages, neutrophils, dendritic cells and monocyte-derived suppressor cells) and lymphoid (mainly natural killer cells, T and B lymphocytes) origin as well as cells comprising blood vessels and lymphatics[3,4]. Examples of least studied, rare or cancer type-specific populations within the tumour niche are adipocytes, mesenchymal stem cells and neurons[5–7]. The complex interactions between cancer cells and allegedly normal, constituent cells together with non-cellular components (the extracellular matrix or ECM) are collectively known as the tumour microenvironment (TME)[4] (**Fig. 1C**). The contribution of vascular cells and angiogenesis in tumour progression has been long appreciated[8].

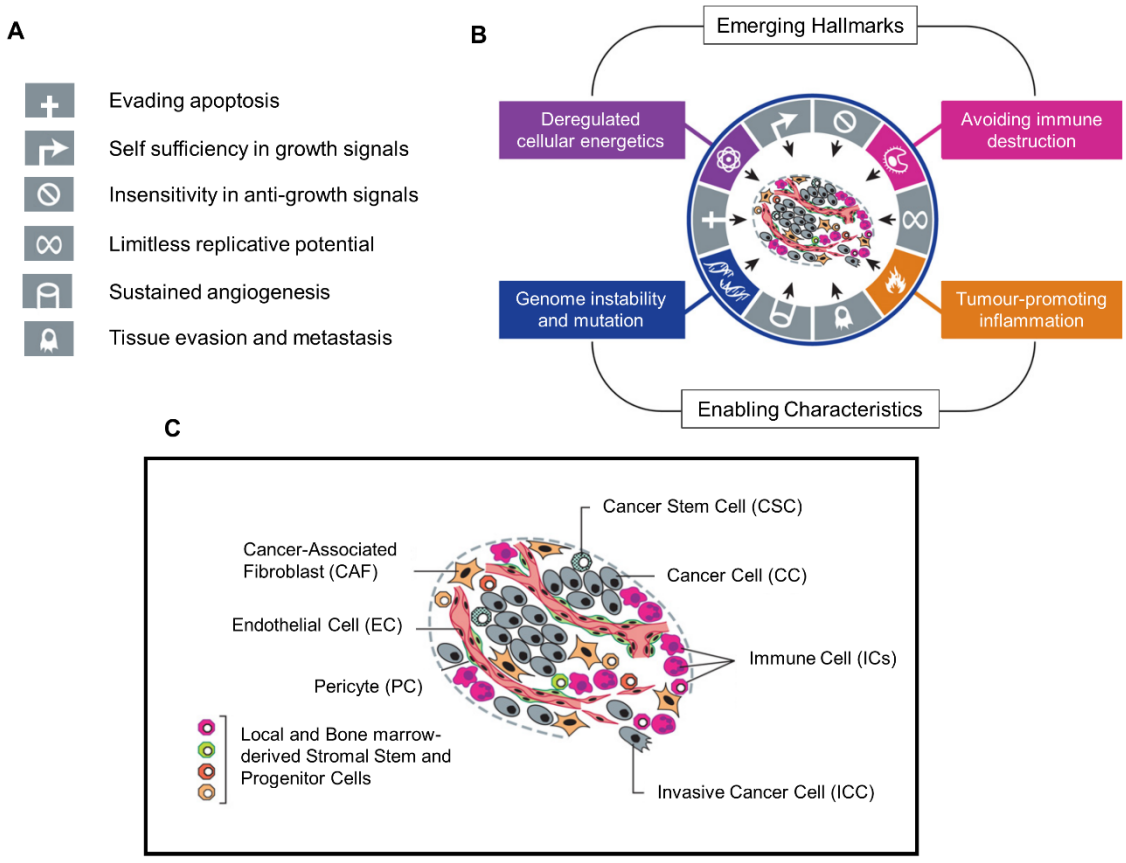

Figure 1. Tumour microenvironment components facilitating the hallmarks of cancer. (A) The first-defined hallmarks of cancer, based on tumour cell ability to (i) proliferate indefinitely (ii) with self-provided growth signals (iii) regardless of inhibitory factors, (iv) resist cell death, (v) evade neighbouring tissue and metastasize. The (vi) sustained angiogenic potential has long been recognized as a key driver of tumourigenic capabilities and signifies the importance of TME-related tumour progression. **(B)** Emerging hallmarks (tumour metabolism and evasion from anti-tumour immunity) and enabling properties (genetic instability/mutation burden and inflammation-mediated tumour promotion) of cancer over the last decade. **(C)** Schematic representation of typical host cell populations within solid tumours. It is important to note that cancer cells themselves constitute a heterogeneous population with distinct abilities of stemness, invasion as well as resistance to therapy[9]. For reasons of simplification, several bone-marrow-derived and mesenchymal cell types and subpopulations are not depicted. *Source: modified from Hanahan and Weinberg 2000, 2011*[1,2].

1.1 Angiogenesis and cancer

Vessel structure and morphogenesis

The vascular system supplies all body regions with nutrients, gases and trophic signals and undertakes the removal of waste and carbon dioxide[10]. Apart from substance exchange, blood vessels have a prominent role in (a) inflammatory response by modulating leukocyte trafficking, (b) hemostasis by regulating the availability of anti- and pro-coagulant mediators, (c) blood flow dynamics and (d) fluid homeostasis[11]. To implement these functions, vascular networks constitute extensive circulatory loops of arteries and veins. Capillaries serve as a connective node within this closed system of blood circulation.

At a cellular level, the vascular wall is composed of distinct components. Endothelial cells (ECs) are key constituents of blood vessel structure and function. ECs form a cobblestone-like monolayer (‘phalanx’) lining the inner-most surface of vessels and they are covered by a continuous, laminated ECM known as basement membrane (or basal lamina). Mural cells (pericytes or vascular smooth muscle cells (vSMCs)) are embedded within the basement membrane and ensheath the abluminal surface of vessels to provide support to the endothelium (**Fig. 2A**). The origin, abundance and composition of mural cells, the specialization of ECs (for example the expression of specific surface molecules and permeability) and the ECM constitution vary among different vessel types and locations[12].

During development, the vascular network represents one of the earliest organ systems formed to address the requirements of the growing embryo (nutrition and trophic signals) and it is initially established by the process of **vasculogenesis** (the *de novo* formation of blood vessels). The first step of the vasculogenic process is the differentiation of splachnopleuric mesodermal cells into haemangioblasts that subsequently aggregate into structures termed as blood islands[13]. Blood islands in the mouse embryo arise approximately at the embryonic day 7.5 (E7.5) in the extra-embryonic yolk sac and are comprised of endothelial precursor cells (EPCs) or angioblasts in the periphery while haematopoietic stem cells (HSCs) are localized inside the lumen. The fusion and remodelling of multiple blood islands lead to the assembly of the honeycomb-like vessel primordia termed as primitive vascular plexus or labyrinth (E8.5) (**Fig. 2B**)[14,15]. Multiple signalling proteins including vascular endothelial growth factors

(VEGF)[16,17], transforming growth factor-β (TGF-β)[18], ephrins[8] and Indian hedgehog protein[19] as well as cell adhesion molecules such as vascular endothelial cadherin (VE-cadherin or CD144) and platelet-endothelial cell adhesion molecule-1 (PECAM-1, PECAM or CD31)[20] have been identified to regulate vasculogenesis. Despite supporting evidence, the existence of post-natal vasculogenesis from bone-marrow-derived cells (BMDCs) and/or resident endothelial progenitor cells remains debated[8,21].

Following the formation of the primitive vascular plexus, additional growth of blood vessels by a process known as **angiogenesis** (the development of new blood vessels from existing ones) emerges approximately on E8.5-E9.5 (**Fig. 2C**)[14]. This angiogenic remodelling establishes the hierarchical organization of the vascular network into arteries, arterioles, capillaries, venules and veins[10,22]. Angiogenesis can be separated into **(i)** intussusceptive angiogenesis which includes the longitudinal splitting of pre-existing vessels into new daughter vessels through intraluminal protrusions of transvascular pillars. Although mechanical stretching[23], haemodynamics[24,25] and signalling (in particular VEGF[26]) have been shown to impact vessel splitting, very little is known about the occurrence and the precise molecular mechanisms of intussusception[27,28]. For this reason, the term 'angiogenesis' in a strict manner refers to the more well-studied **(ii)** sprouting angiogenesis (the branching of new blood vessels from pre-existing ones).

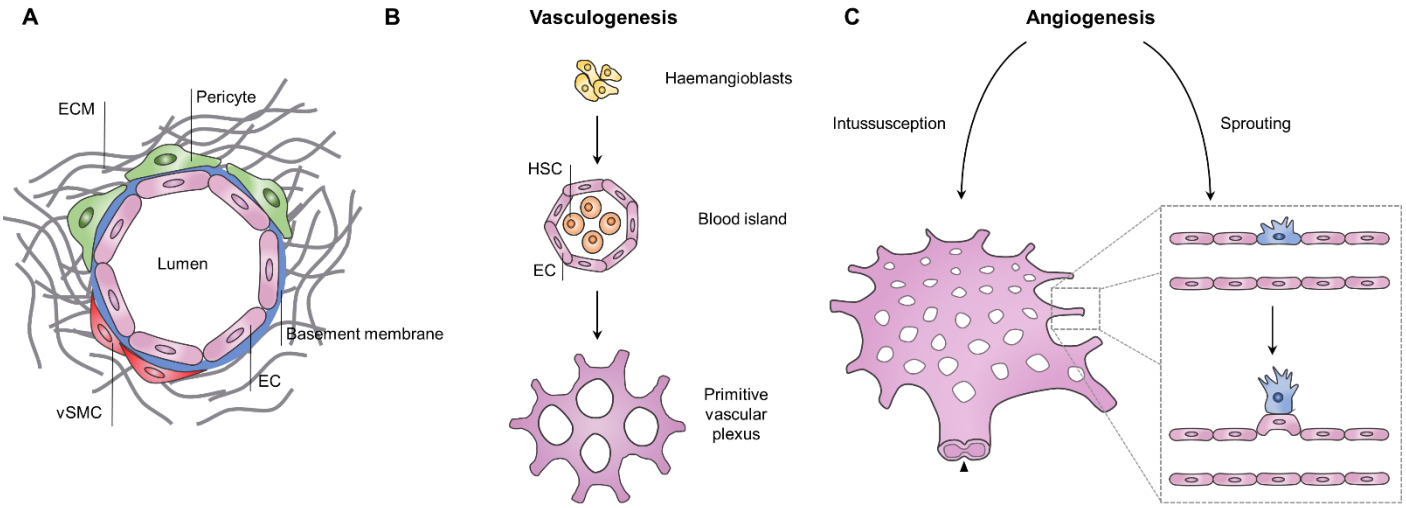

Figure 2. Vascular structure and development. (A) The vessel wall comprises of both cellular (endothelial cells and pericytes or vascular smooth muscle cells) and ECM components. For reasons of simplification, the basement membrane is depicted between ECs and mural cells. In reality, these cells are embedded within the basement membrane. **(B)** In the developing embryo, the first vascular network (primitive vascular plexus) is established by the formation of cell aggregates (blood islands) from mesoderm-derived haemangioblasts. ECs derived from the differentiation of EPCs or angioblasts localize in the outer edges of blood islands. The process of *de novo* vessel formation is defined as vasculogenesis. **(C)** The expansion of the primitive vascular plexus into a highly organized vascular system is accomplished through angiogenic processes. These include the intussusception – the insertion of pillars of vascular tissue inside the lumen leading to vessel bifurcation, and the sprouting angiogenesis – the creation of blind-ended tubes (sprouts). *Source: modified from Kolte et al. 2016*[13]

Cellular and molecular mechanisms of sprouting angiogenesis

During adulthood, the vascular wall remains under a quiescent state in terms of growth and remodelling but ECs are characterized by the outstanding capacity of re-entering into the cell cycle in response to environmental stimuli. Nevertheless, the efficient implementation of angiogenesis requires a sequence of tightly orchestrated morphogenic events and cellular behaviours, as it is discussed in more detail below (**Fig. 3**).

a) Vessel activation: Local hypoxia is key priming of the angiogenic programme, as it promotes the production of pro-angiogenic factors including VEGF and cytokines[29,30]. VEGF-A or vascular permeability factor (VPF) is the dominant mediator of vessel morphogenesis among the angiogenic cues[10,31]. ECM degradation from matrix metalloproteinases (MMPs) contributes to (i) disintegration of the surrounding basement membrane, (ii) generation of anti-angiogenic molecules to hinder inapt branching and (iii) further liberation of pro-angiogenic molecules embedded within the matrix[8,32]. The nascent vessel dilates due to the detachment of mural cells (mainly mediated by angiopoietin-2 (ANG-2)) and loosening of endothelial intercellular junctions[8,22,33]. High permeability leads to leakage of plasma proteins, for example, fibronectin and fibrinogen, and deposition of an interim ECM that serves as a scaffold for cell migration (through integrins)[8]. In response to pro-angiogenic factors, ECs switch from a quiescent phenotype with long half-live to an activated state leading to the initiation of vessel sprouting.

b) Tip cell selection: The ECs that are specified to lead the vessel spouting are called tip cells (TCs). They acquire high motility and they extend finger-like membrane projections (filopodia) that act as sensors of the angiogenic signals. Conversely, cells that trail TCs are less motile ECs with higher proliferative potential termed as stalk cells (SCs)[34]. TC specification is mediated by VEGF signalling, while the formation of SCs is controlled via the Delta-like 4 (DLL4)-Notch pathway[35]. More specifically, increased VEGF-A in the surrounding microenvironment causes one EC to take the lead as a TC by binding to VEGF receptors (VEGFR)[29]. The TC starts to express higher levels of the Notch ligand DLL4 and prevent adjacent ECs from adopting the same phenotype by activating the Notch pathway (lateral inhibition effect)[34]. The features that drive a particular EC to acquire TC fate within a pool of neighbouring ECs remain largely unexplored. It is now increasingly recognized that there are competition and dynamic transition between TC and SC states rather than an acquisition of fixed phenotypes[36–38]. In addition, recent studies have shed light into the parameters that affect TC specification such as the mitotic activity rate[39] and the asymmetric cell divisions[40].

c) TC guidance and sprout elongation: During sprout outgrowth, TCs receive attractive and repulsive signals (such as netrins, semaphorins and ephrins) through filopodia extension and provide the migratory force and the proper guidance towards adjacent sprouting vessels[41]. The implicated molecules, as well as the morphological and functional features of TCs, are reminiscent of the axonal growth of nerve fibers[42]. The less motile but highly proliferative trailing SCs form the trunk of the sprouting vessel,

support elongation and retain a connection with the parental vessel via junctions with phalanx cells[22,34]. The rate and the orientation of SC division are crucial for the efficacy of vessel sprouting because defects in these properties result in abnormal vessel morphogenesis[43,44].

d) Anastomosis and vessel perfusion: SCs have also an essential role in the lumen formation within the newly forming vessel[34]. Different models of lumen morphogenesis have been described depending on the vessel type, location and the model system used. The most representative mechanisms include i) the coalescence of intracellular vacuoles (cell hollowing), ii) the intercellular vacuole exocytosis and iii) the rearrangement of intercellular junctions and repulse (cord hollowing)[28,34,45]. In most cases, the establishment of apicobasal polarity and cytoskeletal rearrangements of SCs have a significant contribution in luminal expansion[22,32]. When a TC identifies its target (another TC from a developing, adjacent sprout), the motile behaviour of TCs is repressed. The creation of stable VE-cadherin junctions between TCs is a fundamental step for the fusion of sprouting vessels ('head-to-head' anastomosis)[28,46]. Moreover, it has been documented that macrophages support anastomosis by acting as cellular bridges between TC contacts[47].

e) Vessel maturation: Following the formation of vessel contacts, the deposition of the basement membrane and changes in EC behaviour (for example repression of proliferation) support the stabilization of the vascular wall[34]. The recruitment and differentiation of mural cells in the newly formed vessel is mediated by a variety of factors including platelet-derived growth factor-β (PDGF-β), ANG-1 and TGF-β, and has a significant contribution in this process[48,49]. Upon initiation of blood flow, sufficient oxygen supply reduces local VEGF-A levels[32,41]. In addition, haemodynamic forces from the inflowing blood re-establish and strengthen EC junctions, further prompting ECs to return in a quiescent state. The vessel maturation includes additional branching re-arrangements and EC specialization depending on the vascular bed structure and function[12,32]. Vessels with improper guidance or poor perfusion are regressed[50].

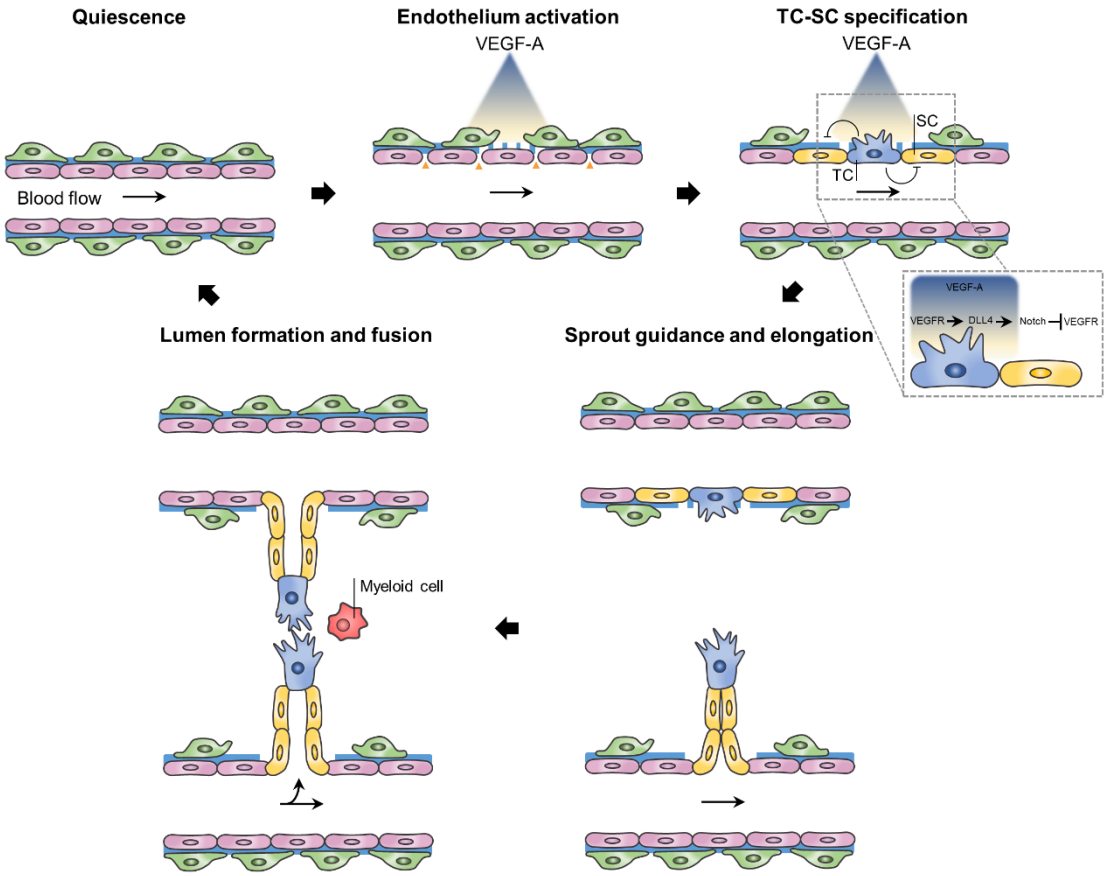

Figure 3. Key cellular and molecular mechanisms of angiogenesis. Under a quiescent state, ECs form a monolayer of streamlined, phalanx cells. Both ECs and pericytes, which cover the abluminal surface of the vascular tube, produce basement membrane components[8]. In the presence of angiogenic stimuli, pericytes detach from the vessel tube and the basement membrane is decomposed, opening tracks for vessel sprouting. The developing sprout is composed of (i) a leading, highly motile TC with filamentous membrane protrusions called filopodia and (ii) trailing SCs with high proliferative capacity that generate the vessel trunk and assist elongation and lumen formation. The DLL4/Notch pathway has a prominent role in TC vs. SC specification. TCs receive guidance from ECM breakdown fragments (haptotaxis) and released signalling factors (chemotaxis) to crawl towards adjacent sprouting vessels[15]. Upon contact between TCs, the newly forming vessels are fused (anastomosis). Myeloid-derived macrophage populations facilitate this process. Following vessel perfusion, a series of remodelling events and changes in cellular recruitment and behaviour leads to the maturation of the nascent vasculature and re-establishment of quiescence. Regression occurs if vessels are poorly perfused.

Normal vs. Tumour vasculature

As noted above, under physiological conditions blood vessels supply tissues with nutrients and oxygen and evacuate metabolic waste products[51]. Cancer discovers ways to gain access to the host vascular network to cover these needs. Besides fueling tumour growth, cancer cells favour neo-angiogenesis to render routes for metastasis[8,32]. Several models of blood vessel formation inside the tumour have been described (**Fig. 4**). Intussusception[52–54] and post-natal vasculogenesis[55] have been documented in solid tumours, but sprouting angiogenesis is the most well-known mechanism of tumour neovascularization[56]. In some cases, cells from the tumour bulk can integrate into the vessel wall (vasculogenic mimicry)[57]. CSCs have also been associated with the formation of tumour-associated vasculature through their differentiation into vascular cells (ECs and/or pericytes) in glioblastoma[58–60]. By contrast, certain tumour

types (such as astrocytoma) hijack the vasculature of the nearby host stroma without promoting vessel growth, a process termed as vessel co-option[61,62]. One or more strategies can be exploited for tumour vascularization depending on the type of malignancy or even the location within the same tumour[63].

Owing to deregulated angiogenic processes, the tumour-associated vasculature is characterized by abnormal structure and function[61,64]. Unlike normal vessels, tumour vessels lack hierarchical organization and have abnormal diameters that vary from extensively enlarged to minute lumens. They exhibit irregular branching, incoherent blood flow (in terms of presence, direction and velocity), aberrant density and shunting[65], establishing a chaotic vascular network with impaired functionality. Defective functional properties include abnormal oxygen supply (promoting tissue hypoxia[66]), leakiness (contributing to interstitial pressure[51]) and altered immune cell extravasation[67,68].

Tumour vessels differ from normal vasculature at all cellular levels. In response to high concentrations of pro-angiogenic factors[6], tumour-associated ECs acquire abnormal morphology developing transcellular holes and intraluminal cytoplasmic projections[69]. They form a multi-layered lining instead of a single layer of endothelium and they are less interconnected by tight junctions (intercellular gaps), contributing to increased tumour vessel permeability and irregular blood flow[70]. Moreover, tumour-associated ECs are characterized by high proliferative capacity[71] and altered metabolism (increased glycolysis)[70,72] in comparison with their normal counterparts. Cytogenetic aberrations such as aneuploidy, chromosomal translocations and irregular centrosomes are also evident in tumour-associated ECs[73]. Owing to their altered properties, tumour-associated ECs positively modulate cancer progression by offering a gateway to tumour cells for metastasis, facilitating immune espace and tumour promoting inflammation (through surface adhesion molecules and chemokine secretion) and obtaining resistance to chemotherapeutic and anti-angiogenic agents [3,69,70].

Pericytes have lower abundance and loose attachment to the tumour vasculature compared to pericytes ensheathing normal vessels. They are morphologically abnormal, extending aberrant protrusions that detach from the vessel wall and orient towards the tumour stroma [71]. Irregular pericyte coverage fails to control angiogenesis and EC proliferation, thus supporting the creation of an abnormal, leaky vascular network with EC hyperplasia and wall fenestrations[70]. Low levels of PDGF-B and excessive expression of VEGF-A are key contributors to incomplete vessel maturation and defective pericyte coverage in cancer but the exact causes remain to be elucidated[6,74]. In contrast to basement membranes that enclose normal vessels, tumour basement membrane constitutes an uneven, multilayered lining of ECM that is loosely attached to ECs and mural cells[69,70].

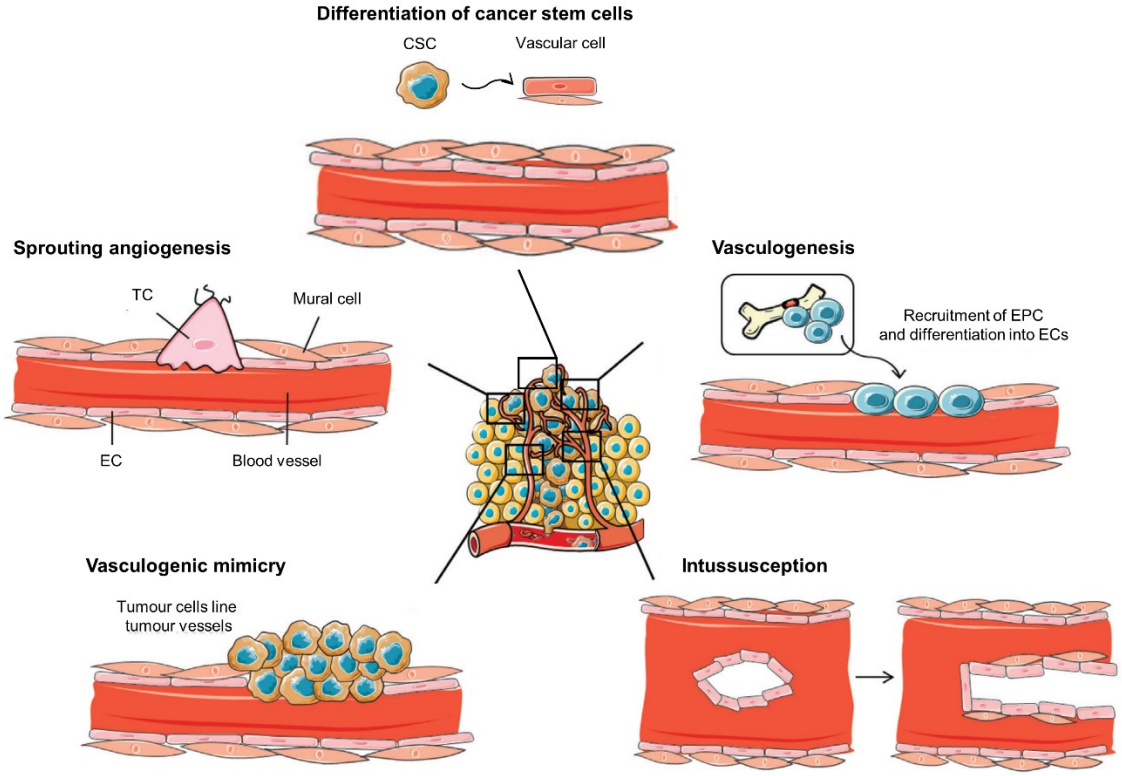

Figure 4. Methods of tumour-associated vessel morphogenesis. Apart from processes that are used also for physiological angiogenesis (vasculogenesis, intussusception and vessel sprouting), tumours have evolved additional strategies to exploit the host vasculature. These include the vasculogenic mimicry (the incorporation of tumour cells into the vascular wall) and the differentiation of CSCs into cellular vessel components, more specifically ECs and/or pericytes. *Source: modified from Zuazo-Gaztelu and Casanovas 2018*[56]

Tumour angiogenesis as a therapeutic target against cancer

The classical view of tumour-associated angiogenesis is separated into two distinct phases: **(i)** an early phase when small-sized tumours (approximately 1-2mm^3) are avascular and concealed, relying on the local host vasculature and entering a dormant state, and **(ii)** a second phase when tumours further grow in size and induce sprouting angiogenesis from nearby existing vessels to facilitate oxygen and nutrient supply and waste removal[61,75]. The transition between these two phases is termed as the **angiogenic switch** and encompasses the prevalence of activators (pro-angiogenic factors) over inhibitors (anti-angiogenic factors) of neovascularization in the angiogenic balance. The tipping of the balance towards pro-angiogenic factors can emerge in any step of tumour development, depending on the tumour type and the TME[61].

Studies over the last decades have pinpointed the major implications of VEGFs in angiogenesis. In mammals, the VEGF family constitutes of five protein members with highly conserved structure (VEGF-A, VEGF-B, VEGF-C, VEGF-D and placental growth factor or PIGF)[76]. Each member mediates biological functions by binding to a specific repertoire of VEGFRs (VEGFR1, VEGFR2 and VEGFR3) and co-receptors (NRP1 and NRP2) with different affinity[77]. Among VEGF family members, VEGF-A is the most studied member that has been linked to angiogenesis promotion both in a normal and a

malignant context[78]. For example, haploinsufficiency (depletion of a single allele) or complete ablation of VEGF-A leads to embryonic lethality due to vascular abnormalities[79,80]. The same applies to VEGF-A overexpression[81], suggesting that even modest alterations can severely impact VEGF-A physiological outcomes. Moreover, most solid tumours have elevated expression of VEGF-A[64]. Therefore, VEGF-A provided the most promising means of targeting angiogenesis for therapy against cancer.

Initial therapeutic strategies aimed to block tumour neovascularization (**anti-angiogenic therapies**) via VEGF-targeting agents which include: **(i)** anti-VEGF antibodies (for example bevacizumab, a prominent agent against VEGF-A), **(ii)** anti-receptor antibodies to hinder VEGF signalling and **(iii)** tyrosine kinase inhibitors of VEGFRs (for instance sorafenib and sunitinib)[75]. Despite promising results in selective tumour types, treatment (either monotherapy or combination treatment with chemotherapeutic agents) efficacy in terms of patient overall survival remains low in multiple cancers[82]. In addition, breaks between anti-angiogenic treatments can lead to rapid tumour-neovascularization and tumour relapse[83]. Acquired resistance to therapy of tumours cells and/or the tumour-associated vasculature has been attributed to several parameters including tumour and vessel heterogeneity, redundancy of pro-angiogenic factors, the complexity of VEGF signalling, tumour stromal cell implications, treatment-induced hypoxia, alternative means of tumour vessel formation and co-option[75,82,84]. Severe toxic effects such as haemorrhaging have also been reported[85].

One additional limitation of anti-angiogenic agents is that vessel destruction impedes drug delivery within solid tumours. Interestingly, preclinical research showed that anti-angiogenic treatment is characterized by an early-occurring, transient window during which tumour hypoxia is alleviated, pericytes are recruited in tumour vessels and cytotoxic therapy is more effective[86]. These observations gave rise to the concept of "**vascular normalization**" by anti-angiogenic therapy that can assist anticancer treatments. This narrow "normalization" window was further detected in a subset of cancer patients[87]. One crucial challenge of this approach is the identification of the appropriate timing and dosing of anti-angiogenic agents in combination with anticancer therapy to achieve sustained vessel normalization and potent drug distribution.

Notably, a recent study from Wong and colleagues proposed that pro-angiogenic strategies can provide a significant solution in cancer therapy[88]. More specifically, the authors showed that low-dosing combination of Cilengitide (αV integrin inhibitor – originally used as an anti-angiogenic agent inducing EC apoptosis in high doses) and Verapamil (calcium channel blocker – vasodilator) promotes the formation of more functional vessels within tumours of preclinical models[89]. Concomitantly, this therapeutic regime induces tumour-suppressing effects similar to "vascular normalization" approaches, including a decrease in tumour hypoxia and enhancement of chemotherapy delivery, with fewer side effects[90] (**Fig. 5**). These findings put "**vascular promotion**" therapies forward for cancer treatment and can potentially offer outcomes of high clinical value in the future.

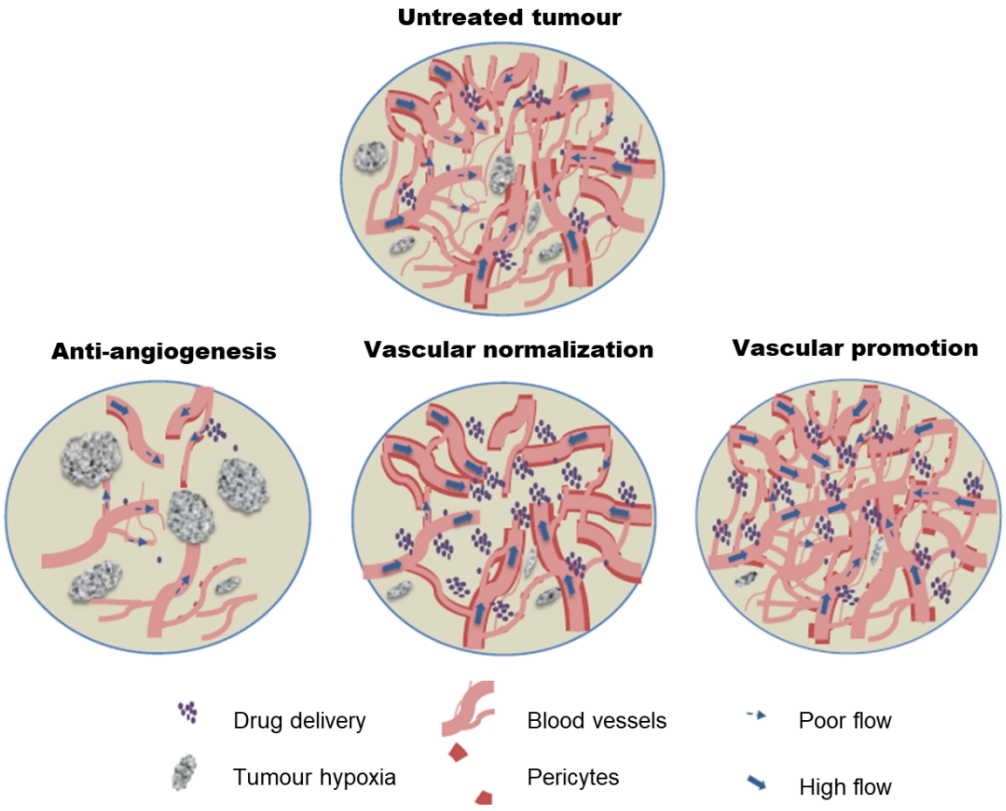

Vascular features	Anti-angiogenesis	Vascular normalization	Vascular promotion
Blood vessel density	↓↓	↓ or ns	↑
Blood flow	↓	↑	↑
Leakiness	↓	↓	↑
Tumour hypoxia	↑↑	↓	↓
Drug delivery	↓	↑	↑
Drug resistance	↑	↓	↓

Figure 5. Therapeutic approaches targeting tumour angiogenesis. Tumour vasculature consists of non-hierarchical networks of vessels with deficient blood flow and pericyte coverage. Although anti-angiogenic therapies have provided favourable clinical outcomes in certain types of cancer, caused vessel destruction can promote pro-tumorigenic conditions such as tumour hypoxia and can impede drug delivery. Under specific dosing, anti-angiogenic treatments can induce vessel normalization within a narrow time frame, resulting in decreased hypoxia, augmented pericyte recruitment, increased blood perfusion and improved drug distribution. Vessel density is decreased or unaffected using this therapeutic regime. A recent approach termed as "vascular promotion" therapy supports the formation of more functional vessels to facilitate anticancer drug efficacy. Indicative alterations in vascular features caused by each therapeutic strategy are summarized in the table below the graphical representation (arrowheads denote increase or decrease of a corresponding feature; ns: no significant difference). *Source: modified from Wong et al. 2016*[82]

1.2 Integrin receptors

The integrin family constitutes a diverse group of single-spanning transmembrane (type I) receptors. They form non-covalently linked heterodimers of α and β subunits that bind to extracellular ligands, including ECM components and immunoglobulin superfamily proteins. In mammals, 18 α and eight β subunits have been identified, forming at least 24 heterodimeric combinations[91]. Among them, half are composed of β1 integrin and five contain av subunit[92]. Each integrin heterodimer has a variable level of specificity for different ligands (for example considering the specificity of α5β1 for fibronectin versus the extensive collection of αVβ3 ligands)[93]. On the other hand, a single ligand can bind to a multitude of integrin receptors. The intracellular interactions in proximity with integrin cytoplasmic tails add on the complexity of integrin-related signalling. These vast molecular associations render integrins crucial mediators of cell survival, adhesion, migration and differentiation in both physiological and pathological conditions[94]. The impact of integrins in tumour progression[93,95–97] and, in particular, tumour angiogenesis[98–100] has also been comprehensively reviewed.

Integrins are in charge of transmitting environmental signals through the plasma membrane by forming a connective node between the extracellular matrix and the intracellular compartment (**Fig. 6**). Initially in an inactivated (closed) state, integrin subunits are bent towards the cell site and have low affinity for binding ligands. Upon ligand engagement, integrins undergo conformational changes and acquire an activated form that enables downstream signalling[93]. During activation, integrins respond to intracellular molecules attaching on their cytoplasmic regions to get a fully extended (open) structure (**inside-out signalling**). Talin protein through the RAP1-RIAM axis and kindlins are well-established activators of integrin receptors[101,102].

Further adhesion and integrin clustering on the cell surface leads to the subsequent formation of multiprotein, adhesion complexes surrounding integrin cytoplasmic tails (termed as **integrin-associated complexs or IACs**) that modulate downstream signalling pathways and anchor cytoskeletal components (**outside-in signalling**)[96]. Therefore, despite the lack of catalytic activity, integrins recruit a variety of kinases (such as focal adhesion kinase or FAK and Src kinases), actin-binding proteins (for example parvins, talin, kindlins, vinculin and α-actinin) and adaptor molecules (like paxillin, integrin-linked kinase or ILK and PINCH protein) that function as a molecular hub between the ECM and the cytoskeleton[96]. Integrin inactivation and IAC disassembly are accomplished via inactivating proteins such as integrin cytoplasmic domain- associated protein 1 (ICAP-1) and SH3 and multiple ankyrin repeat domains (SHANK) proteins.

Before reaching the cell membrane, integrins are heterodimerized in the endoplasmic reticulum and acquire post-translational modifications within the Golgi apparatus[103]. Afterwards, integrins follow a constant turnover cycle by endocytosis and membrane recycling[93]. Interestingly, recent studies showed that integrins maintain their active form as well as associated protein complexes and transmit signals while tethered in endomembrane structures (**inside-in signalling**)[104–106].

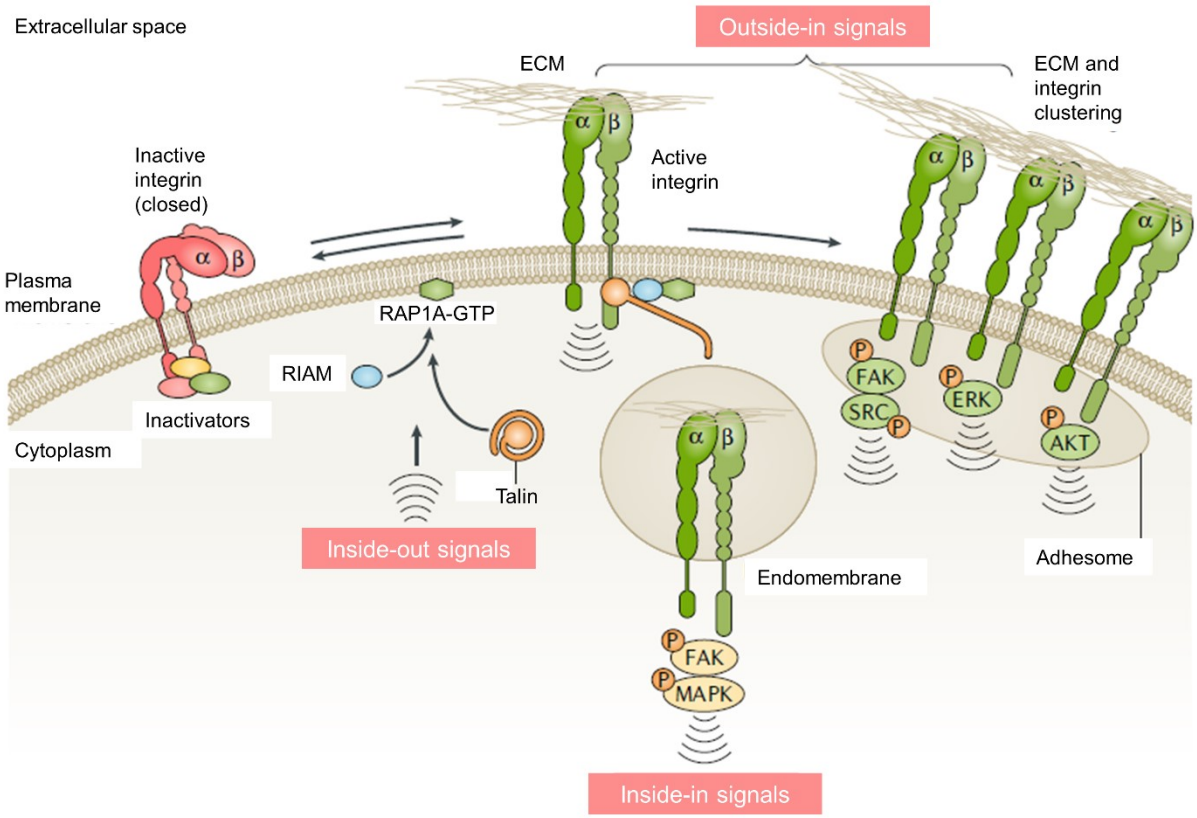

Figure 6. Multiple facets of integrin-mediated signalling. Integrins are type I cell surface receptors with an extended extracellular domain, a single-pass transmembrane region and a short (30 to 40 amino acids long except β4 integrin) cytoplasmic tails[100]. On the cell surface, integrins can acquire different conformations: inactive (closed) and active (extended-closed and extended-open with low and high ligand affinity, respectively)[107]. Depending on the activation state, integrins form distinct protein complexes (IACs; inactive: disorganized and dispersed clusters; active: organized and aligned clusters) in association with their cytoplasmic compartment that mediate outside-in and inside-out signalling. Of note, integrins can perform signal transmission away from the plasma membrane (inside-in signalling). Type I definition: N-terminus region on the extracellular site with removed protein localization signal. *Source: modified from Hamidi and Ivaska 2018*[93]

1.3 The integrin-mediated adhesion network

To carry out multidirectional signalling, integrins recruit multiple proteins near their cytoplasmic domains to compose IACs. IACs form a molecular bridge between the extracellular environment and the cytoskeleton and are essential for tissue development and integrity[108]. Within the cell, apart from environmental sensing of chemical signals (based on the ECM ligand composition and availability of growth factors), IACs integrate multiple physical cues (such as matrix rigidity, dimensionality and distance between ECM ligands)[109]. Therefore, cells manage to respond to a variety of external stimuli by adjusting cellular shape, re-organizing cytoskeletal components and modifying IAC structure and function[110]. Different types of IACs have been described including[108–112]:

(1) Focal complexes or nascent adhesions. They are the first integrin-related structures that can be visible under the light microscope, representing small-sized dots (approximately 100nm in diameter) that are developed transiently underneath membrane protrusions (lamellipodia- thin, wave-like structures of the

cell membrane- and filopodia). Focal complexes are comprised of a few hundreds of proteins (in particular talin and paxillin).

(2) Focal adhesions (FAs). This is the most studied type of integrin-based adhesions. FAs tether on the ends of actin stress fibres (bundles of parallel actin filaments containing filamentous actin and myosin) and mediate stable attachment on substratum and integrin-related signalling. They arise from nascent adhesions following alterations in size/length, protein recruitment (for example zyxin), post-translational modifications and an increase of turnover rate, typically where cell surface extensions retract.

(3) Fibrillar adhesions that are elongated ECM contacts emerging from FAs and appear predominantly in fibroblasts. They localize closer to the cell centre and are mainly formed in tandem with fibrillar matrix such as fibronectin. Fibrillar adhesions are characterized by increased tensin levels and decreased events of tyrosine phosphorylation.

(4) Podosomes. Podosomes are dot-like, adhesion structures with a distinctive actin-rich core and a surrounding ring of integrins and adaptor proteins including talin, zyxin and paxillin. Another unique feature of podosomes is the ability to degrade the ECM through MMP secretion. Podosomes are found in several cell types including macrophages, dendritic cells, osteoclasts, vSMCs and ECs.

(5) Invadopodia. This adhesion type is structurally and functionally similar to (yet larger in size than) podosomes. Invadopodia are formed in virus-transformed fibroblasts and malignant cells in fewer numbers per cell compared to podosomes.

To unravel the complexity of IAC molecular composition, *in silico* studies spanning the last decade have determined and elaborated the **integrin "adhesome"**. Zaidel-Bar et al. (2007) first defined a comprehensive network of 156 components (151 proteins and four lipids and calcium ions) with an intrinsic (scaffolding) core and transiently associated (effector) molecules. Interestingly, approximately 700 interactions were mapped on the adhesome, reflecting the complex nature of integrin-mediated signalling[113]. Based on experimental studies, this network was further refined with 232 components comprising the "literature-curated integrin adhesome"[108]. More than half adhesome molecules were found to be regulated via defined "switches" (changes in interaction partners, conformation, phosphorylation, protein cleavage and phospholipid binding)[114]. In a milestone study, computational integration of seven IAC proteomics datasets generated a 2.412-protein nexus termed as the integrin "meta-adhesome"[115]. The authors then established a consensus of 60 proteins (**Fig. 7**) as a potential IAC core with context-independent presence ("**consensus adhesome**") that can be subdivided into four axes (based on the prevalence of these proteins on literature reports and the already published nanoscale architecture of IACs[116])[115,117]:

- The zyxin and α-actinin family member module
- The talin, vinculin and vinculin-binding protein (ponsin and vinexin) layer

- The FAK and paxillin axis
- The kindlin and **ILK-PINCH-Parvin (IPP) complex** module

The composition and organization of the integrin adhesome are continuously upgraded with the characterization of novel members and refinement of interactions. Despite significant advances in super-resolution microscopy, -omics approaches and bioinformatics tools, crucial challenges revolving around the adhesome functionality remain considering the variability between different cell types, dimensions (2D versus 3D cultures), integrin heterodimers and structures of IACs. However, accumulating evidence suggests that the impact of integrin adhesome expands on "distal" cellular processes such as the cell cycle checkpoints, cytoskeletal re-arrangements during cell division and cell metabolism (beyond the effect on cell motility, survival and differentiation)[118].

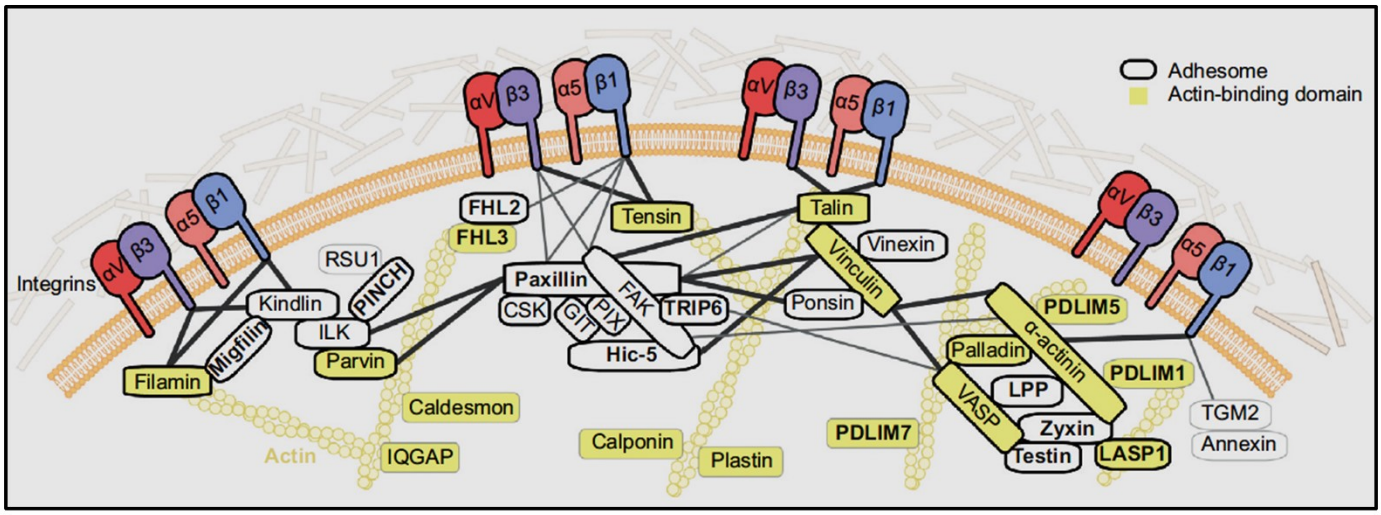

Figure 7. The integrin consensus adhesome: The core adhesion molecules that are commonly found in FN-induced IACs (enriched in at least five out of seven proteomics datasets deriving from human cancer cells -melanoma and erythroleukemia cells-, and human and murine fibroblasts). The consensus adhesome contains both well-established and previously undefined integrin adhesion components. Underappreciated consensus molecules (18 proteins) without network interactions are not presented in the graph (ALYREF, BRIX1, DDX18, DDX27, DIMT1, DNAJB1, FAU, FEN1, H1FX, HP1BP3, LIMD1, MRTO4, P4HB, POLDIP3, PPIB, RPL23A, SIPA1 and SYNCRIP). The thickness of the grey links corresponds to the experimental validity of each interaction. Additional indications: yellow colour, actin-binding protein; bold text, LIM domain-containing protein (explained below); thick black border, protein reported in the "literature-curated integrin adhesome". *Source: Horton et al. 2016*[119]

The IPP complex

The ternary complex of ILK, PINCH and parvin is a consensus adhesome component that couples integrins with the cytoskeletal compartment and serves as a signalling centre within IACs. **Particularly interesting new cysteine-histidine-rich protein** (**PINCH**) consists of five LIN-11, Isl1 and MEC-3 (LIM) domains followed by a short C-terminus tail[120]. Two PINCH isoforms (**PINCH1** and **PINCH2**) have been described with 82% sequence homology (in human) that are encoded by two separate genes (*LIMS1* and *LIMS2*)[121]. **Integrin-linked kinase** (**ILK**) is a single isoform pseudokinase that contains an N-terminus region with ankyrin (ANK) repeats, a C-terminus kinase domain (that lacks catalytic activity of Ser/Thr protein kinase[122]) and an internal pleckstrin homology (PH)-like motif. The N-terminus LIM1

domain of PINCH interacts with ILK via the ANK repeat domain. Moreover, the ILK C-terminus domain associates with the second out of two calponin homology (CH) domains of **parvin** which is localized in the C-terminus region. Parvin family contains three isoforms (encoded by three different genes) in mammals, namely α-parvin/actopaxin/CH-ILKBP and the least studied β-parvin/affixin and γ-parvin.

Of note, studies during the last decades have demonstrated that the formation of IPP complexes in mammalian cells **(i)** takes place before the translocation within integrin-based adhesions, **(ii)** is a prerequisite that enables each member of the complex to localize within IACs, and **(iii)** governs the stability of IPP members against proteasomal degradation[123,124]. Initial *in vitro* experiments in several cell types (using molecular inhibitors, expression of genetic constructs and RNA interference) as well as genetic manipulation of common model organisms (mainly *Caenorhabditis elegans*, *Drosophila melanogaster* and mice) revealed that the IPP structural basis is a key regulator of cell survival, proliferation, motility and ECM deposition[125]. Although IPP proteins appear to function in synergy, there is increasing support for each member of the complex having individual functionalities[125,126] according to representative indications:

1) IPP complex members differentially interact with molecular partners. For example, ILK connects with β integrin cytoplasmic tails directly or indirectly through kindlin-2 (although direct interaction seems to have a cell-type-specific presence in mammals[126]). Parvins are capable of binding to filamentous actin directly or via paxillin and α-actinin[124]. Moreover, PINCH1, but not PINCH2, forms specific links with Ras suppressor-1 (RSU-1)[127].
2) Deletion of ILK[128], PINCH1[129] or parvin[130] in mice leads to embryonic lethality, yet in different staging of embryo development. In particular, both ILK and PINCH1 deficient mice show disrupted development in the peri-implantation stage but different embryonic day (E) death timepoint (ILK: E5.5-E6.5; PINCH: E6.5-E7.5). Developmental defects and embryo death caused from α-parvin deletion occur later (E10.5 and E10.5-14.5, respectively). Of note, β-parvin[126], γ-parvin[131] and PINCH2[132] null-mice exhibit no apparent phenotype.
3) The binding of PINCH isoforms and parvin isoforms in ILK is mutually exclusive[121,124] and their expression patterns overlap in a variety of mammalian tissues[133] (except for γ-parvin which is more specific for the haematopoietic system[134]). Therefore, multiple combinations of IPP complexes can be formed within the same cell, potentially facilitating different functions. The distinct role of different IPP complexes can be supported from the fact that suppression of each separate component does not result in identical phenotype within the same cell type used *in vitro*[135,136] and embryoid bodies[137].

1.4 PINCH in normal function and cancer

The crucial role of PINCH in development was initially demonstrated in lower organisms (expressing only one single PINCH isoform) which exhibited muscle attachment defects[138,139]. Constitutive PINCH1 loss-of-function is embryonic lethal in all metazoan species tested (worm, fly and mouse). In particular, PINCH1 depletion in mice and embryoid bodies results in disrupted epiblast polarity, defective cavitation, endoderm detachment as well as abnormal cell-cell junctions and elevated endodermal cell apoptosis[140]. To avoid embryonic lethality, transgenic tools for the generation of conditional knockout animals were used and elucidated the impact of PINCH in specific tissues *in vivo*. For example, inactivation of PINCH1 from murine epidermis causes progressive alopecia, blisters and epidermal hyperthickening[141]. Deletion of PINCH1 or PINCH2 in cardiac muscle does not result in any overt phenotype at basal level[129,142]. Nevertheless, in mice subjected to myocardial infarction, loss of either PINCH1 or PINCH2 impedes cardiac function[142]. Deficiency of both PINCH1 and PINCH2 in murine myocardium leads to postnatal lethality within four weeks due to heart failure[142]. Redundancy between isoforms was also observed in a recent study focusing on the role of PINCH in bone homeostasis. Mice lacking PINCH1 and PINCH2 from osteocytes and mature osteoblasts show increased loss of bone mass and adiposity while single PINCH deletion does not show any severe osteopenia[143]. This phenotype is attributed to PINCH-mediated regulation of osteoblast differentiation, osteocyte apoptosis and bone mechanotransduction[143]. Of note, global PINCH2 deletion together with hepatocyte-specific PINCH1 loss in mice induce hepatic tissue abnormalities, increased liver size and spontaneous tumorigenesis[144]. Despite the importance of ILK[145–147] and α-parvin[130,148] in **murine endothelium** function *in vivo*, the effect of PINCH in EC biology remains unresolved.

Based on the impact of this integrin adaptor in tissue development and maintenance, recent evidence implicate PINCH in disease including cardiomyopathy, HIV, renal disease and, particularly, cancer[149,150]. The expression of PINCH1 and PINCH2 has been found upregulated in **tumour-associated stromal cells** of common human malignancies (skin, prostate, colon, lung and breast carcinomas), notably in tumour-invasive edges[151]. Moreover, increased PINCH expression within tumour niche has been associated with poor prognosis in colorectal cancer[152]. Increased PINCH expression was further defined in gliomas[153,154], oral squamous cell carcinomas[155], and gastric adenocarcinoma[156]. Although the above body of literature indicates a direct correlation between PINCH and cancer, mouse models to dissect the role of this integrin adaptor in distinct tumour stromal components are still lacking.

1.5 Project aims

In this project, we aim to explore the impact of **PINCH1** (the first-described member of PINCH family) on **tumour-associated vasculature** *in vivo* by addressing **three objectives**: **(1)** Assess tumour growth of two different subcutaneous tumour models (tumours emanating from lung adenocarcinoma or

melanoma murine cancer cells) in mice **(2)** Explore the role of PINCH on tumour-associated blood vessels by defining vessel number, size, structure and functionality. **(3)** Investigate the impact of EC PINCH1 deletion on additional TME components including pericytes, fibroblasts and immune infiltrate. EC-specific PINCH1 ablation resulted in decreased growth of lung adenocarcinoma tumours, with less leaky tumour-associated vasculature. On the other hand, knockout (KO) melanoma tumours showed similar development and vessel functionality to wild type tumours. PINCH1 deletion in ECs did not strikingly affect tumour-associated vessel density and structure. To overcome **isoform-specific compensation**, we verified PINCH2 expression by ECs and generated double PINCH KO tumour-bearing mice. Complete PINCH ablation from ECs led to decreased volume of lung adenocarcinoma-derived tumours and appears to reduce tumour vessel number. Together, our work provides meaningful observations into the functional impact of PINCH1 and PINCH2 on the tumour vasculature using murine tumour models and imaging technology.

The second aim of this study was to investigate whether local RNA translation occurs in FAs of ECs. An in-house protocol for FA isolation using a protein crosslinker and RIPA buffer (protocol 1) produced small amounts of low-quality RNA. Additional protocol modifications (RNA crosslinking and proteolytic degradation) did not improve RNA yield and purity. Therefore, we standardized a FA isolation protocol using a mild lysis buffer (protocol 2) to manage isolate sufficient RNA in terms of quantity and integrity. These findings imply that RNA is localized in FAs of ECs and can shed light into **integrin-mediated translation mechanisms**.

2. MATERIALS AND METHODS

Resources

Detailed lists of antibodies, assay kits, chemicals, primers, cell lines and software used are available in supplemental material.

Mice

All procedures and experimental protocols were performed under the approval of the BSRC "Alexander Fleming" Project Evaluation Committee. The conditional *PINCH1* and *PINCH2* null alleles (floxed alleles) were constructed by gene targeting in embryonic stem (ES) cells that resulted in the insertion of loxP sites flanking the exon 4 [140] and exons 3 and 4 [132], respectively. To achieve conditional endothelial-specific *PINCH* deletion, mice carrying loxP-flanked *PINCH* genes ($PINCH^{fl/+}$ and/or $PINCH^{fl/fl}$) were crossed to *Pdgfb*-Cre/ERT2 mice [157]. To monitor the efficacy and specificity of the Cre-loxP system, the *mT/mG* (or mTmG) reporter transgene encoded by a ubiquitous promoter (ROSA26 or ROSA) was used on occasion.

Syngeneic mouse tumour models

For *in vivo* tumour growth studies, age- and sex-matched littermates were used (8-weeks old, males, C57BL6 background). The mouse tumour cell lines CMT19 (lung adenocarcinoma) and B16F0 (melanoma) were used for syngeneic implantation. Tamoxifen was administered by oral gavage in three doses (4mg, 2mg, 2mg per adult) to induce satisfactory Cre recombinase activity. Endothelial-specific *PINCH* null and wild-type mice were anesthetized with 2.5% isoflurane and 2×10^6 cancer cells suspended in Phosphate-Buffered Saline (PBS) were subcutaneously injected into the flank. Twelve, fourteen or twenty days after inoculation, mice were euthanized in CO_2 or perfused with 4% paraformaldehyde (PFA) fixative (described below) and tumours were harvested. To examine blood vessel functionality and perfusion, mice received intravenous injections of 3 mg FITC-conjugated dextran (2000 kDa) in PBS 30 minutes before euthanization. After excision, tumour dimensions were measured using a caliper. Tumour growth was estimated with the formula length × height × width × 0.52. Tumours were either (1) snap-frozen in liquid nitrogen and maintained at -80°C until used or (2) fixed in 4% PFA at 4°C overnight, PBS washed and dehydrated in 30% sucrose.

Whole animal perfusion

To improve preservation of tumour tissue for immunofluorescence procedures, mice were deeply anesthetized with a ketamine/xylazine cocktail administered through intraperitoneal injections. Following complete anesthesia (assessed by pedal reflex), mice were surgically opened through diaphragm dissection to access the rib cage. The thoracic cavity and the heart were exposed with one

horizontal and two lateral incisions to the rib cage. After a cut in the right atria, 4% PFA (6ml) was administered in the left ventricle of the beating heart at a slow and steady pace. Perfusion success was assessed with the clearing of the liver and fixation tremors.

Genotyping

To maintain transgenic and wild-type animal colonies, the genetic identity of mice was assessed through DNA isolation and subsequent polymerase chain reaction (PCR) experiments. Mice 8-10 day of age were marked though toe clipping using sharp scissors. Toe tissue was incubated in 100μl of lysis buffer (50mM Tris-HCl pH=8.5, 10mM EDTA pH=8.0, 100mM NaCl, 0.2% SDS) containing 0.1 mg/ml proteinase K at 55^{o}C overnight. The DNA was then extracted by adding 6M NaCl (50μl) and equal volume of isopropanol. Samples were centrifuged at 13.000 rpm for 20 min and the supernatant was discarded. For ear biopsies (experimental adult mice identification), samples containing NaCl were centrifuged at 13.000 rpm for 20 min and the supernatant was transferred in a clean 1.5mL eppendorf tube. Equal volume of isopropanol was added and centrifuged again at 13.000 rpm for 20 min. After washing with 70% ethanol, the pellet was air-dried and diluted in 100 μl water for injection (WFI). The genetic make-up of mice was evaluated through conventional PCR amplification. For the PCR reaction, a 20μl mixture was prepared containing 10μM primers (1μl per primer), 10× Taq buffer (500mM KCl, 100mM Tris-HCl pH=8.8, 15mM $MgCl_2$, 0.8% NP-40) (2μl), 25mM $MgCl_2$ (0.8μl), 100mM deoxy-nucleotide triphosphates (dNTPs) (0.2μl), Taq enzyme (0.5-1μl), 1μl of extracted DNA and WFI. Amplification was performed using a thermocycler (PTC-0200 DNA Engine Cycler, Biorad) with the following programme: 3-5 min at 94-95^{o}C; 34-35 cycles with 30-45 sec at 94-95^{o}C, 30-60 sec at 56-61^{o}C, 45-60 sec at 72^{o}C; 2-5 min at 72^{o}C. PCR samples were mixed with 6× DNA loading dye (0.4% bromophenol blue, 0.4% xylene cyanol, 50% glycerol) and migrated in 1.5% agarose gel with 1× Tris Acetate EDTA (TAE) running buffer at 120V. Ethidium bromide staining (1:10.000 dilution) was used for band visualization with UV light.

Flow cytometry in tumour samples

For FACS analysis, tumours were dissected and skin was completely removed. Next, minced tumours were cut into pieces and digested in collagenase, DNase, dispase, 3mM $MgCl_2$ Dulbecco's PBS (DPBS) solution for 30 min at 37^{o}C with manual shaking every 10 min. Remaining tumour tissue was mechanically homogenized using a syringe with 18G needle and a cell strainer. Fetal Bovine Serum (FBS) was used for digestion enzyme inactivation. Cell populations were pelleted by centrifugation for 3 min at 1400rpm, resuspended in 10mL DPBS with 2% FBS and counted manually using a Neubauer chamber. In a 96-well V-bottom plate, 2-4 × 10^6 cells were plated per well and centrifuged for 5 min at 1200rpm. The anti-Fc Receptor (anti-CD16/32) antibody (1:100) was used to avoid non-specific binding. Cells were then incubated with fluorescent-conjugated antibody against PECAM for 30min to 45 min on ice. Cells were washed with DPBS/2% FBS. To stain for intracellular markers, cells were

incubated in Fixation solution (Fix and Perm kit) for 15 min and then incubated with the Permeabilization medium for 10 min at room temperature. Cells were then incubated with primary antibodies against aSMA or vimentin in Permeabilization medium for 30 min at room temperature. Cells were washed twice with Permeabilization medium and incubated with Cy5 anti-mouse secondary antibody for 30 min at room temperature. Labelled cell populations were analyzed by FACS Canto II flow cytometer.

Staining in mouse tumour sections

To study the tumour-associated vasculature and additional TME components, tumours were embedded in OCT and dissected using a Leica CM 1950 cryostat. Midline thick (50μm) cryosections were fixed in 4% PFA for 10 min, washed in PBS two times and permeabilized with 0.5% Triton X-100 in PBS for 30 min in room temperature. After PBS washing, sections were blocked in 1% Bovine Serum Albumin (BSA) in PBS for 1h in room temperature and incubated with primary antibodies in blocking solution at 4^{o}C overnight. Sections were then rinsed in PBS and incubated with Alexa Fluor- or CF- conjugated secondary antibodies and 4′,6-diamidino-2-phenylindole (DAPI; 1:1000) for 1h at room temperature. Specimens were rinsed and mounted using anti-fade mounting medium containing 2.5% 1, 4-Diazabicyclo-octane (DABCO), 10% Mowiol 4-88, 25% glycerol and 0.1M Tris-HCl (Mowiol mounting medium).

Image analysis using confocal microscopy

Images of thick mounted sections were acquired using a laser scanning confocal microscope (Leica TCS SP8 X) to generate z-stacks (z-step size: 1.1-5μm) and analysed with the IMARIS software. To determine vessel size, the surface of the PECAM or the mTmG signal was measured. The area of each individual vessel was calculated using the vantage option (scale: 0.01, offset: 0.00). The number of blood vessels per microscopic field was also estimated. To investigate pericyte coverage, the vessel (primary surface) and the NG2 positive (secondary surface) surfaces were determined. The contact surface area was defined as the area above the primary surface where the primary and the secondary surface physically overlap. The % surface area coverage is calculated using the formula: contact surface area / primary area × 100. Similar approach was followed to calculate the co-localization area in dextran-PECAM stained sections. Images with CD68 and CD3 staining were analysed on ImageJ using the Threshold and Multi-point function, respectively. All double-stained images were recoloured to magenta-green figures to be more accessible to readers with red-green colour-blindness.

Immunofluorescence and quantification of blood vessel density

To examine the number of blood vessels, midline thin (10μm) cryosections were fixed in 4% PFA for 10 min, washed in PBS two times and permeabilized with 0.3% Triton X-100 in PBS for 10 min in room temperature. After PBS washing, sections were blocked in 1% BSA in PBS for 1h in room temperature

and incubated with anti-PECAM primary antibody in blocking solution at 4°C overnight. Sections were then rinsed in PBS and incubated with anti-rat Alexa Fluor 488- or 546- conjugated secondary antibodies and DAPI for 1h at room temperature. Specimens were rinsed and mounted in Mowiol mounting medium. Tile scans of mounted sections were acquired with a 10× objective using fluorescence microscopy. Images were stitched using the ZEISS ZEN microscope software. The total number of blood vessels per tumour area was measured using ImageJ.

In vitro cell culture

All cell lines were grown as monolayer cultures at 5% CO_2, 37°C and 95% humidified cell culture incubator. Mouse tumour cell lines and non-EC cells were cultured in Dulbecco's modified Eagle's medium (DMEM) supplemented with 10% FBS, 1% Penicillin/streptomycin and 1% GlutaMAX. Immortalized mouse lung endothelial cells were maintained in a 1:1 mixture of DMEM and Ham's F-12 supplemented with 10% FBS, heparin (50µg/mL), L-glutamine stable (2mM), endothelial cell growth supplement (0.0125mg/mL) and antibiotics. Non-immortalized, primary cells were isolated and cultured as previously described[158]. Tissue culture plates and coverslips for all EC experiments were coated using a collagen I (30 µg ml^{-1}), gelatin (0.1%) and fibronectin (10 µg ml^{-1} for primary cells, 5 µg ml^{-1} for immortalized cells) coating matrix. Cells reaching 70-80% confluency were detached from the surface using 0.025% Trypsin/EDTA and passaged (at a ratio of 1:4 or 1:5 for immortalized and cancer cells). Alternatively, cells were cryo-preserved in the respective cell culture medium/10% DMSO in liquid nitrogen.

Flow cytometry

To label cells for endothelial cell surface markers, cells were dissociated with trypsin and resuspended in DPBS) containing 0.1% BSA. Cells were then incubated with primary antibodies against ICAM2, PECAM or fluorescent-conjugated antibody against VE-cadherin for 30 min on ice. Cells were then washed twice with DPBS/0.1% BSA and incubated with Alexa Fluor 633-conjugated secondary antibody as appropriate. Labelled cell populations were analyzed by FACS Canto II flow cytometer.

Immunofluorescence staining

Cells (2×10^4) were seeded on coated 13mm glass coverslips and fixed in 4% PFA for 10 min at room temperature. Thereafter, cells were washed two times with PBS, permeabilized with 0.2% Triton X-100 in PBS for 10 min and then blocked in PBS with 1% BSA for 1h at room temperature. Cells were then incubated with anti- PECAM1 and anti-vinculin 1 antibodies overnight at 4°C. Cells were then rinsed in PBS and incubated with Alexa Fluor- or CF- conjugated secondary antibodies and DAPI (1:1000) for 1h at room temperature. Specimens were rinsed and mounted on microscope slides using Mowiol mounting medium. Mounted cells were analyzed by fluorescence microscopy using a Leica DFC345 FX camera and a Leica DM2000 microscope.

Quantitative real-time PCR

RNA was extracted using the RNeasy Mini Kit according to the manufacturer's instructions or with Trizol (described below). RNA concentration was determined using the Nanodrop ND-1000 Spectrophotometer (ThermoFisher Scientific). RNA quality was assessed by A_{260}/A_{280} and A_{260}/A_{230} ratios, indicative of protein and residual chemical contamination respectively. A ratio ≥ 2,0 is generally considered as high purity RNA. RNA integrity was evaluated through electrophoretic separation on 1% agarose gel. cDNAs were synthesized by using the RevertAid or SuperScript III First Strand cDNA Synthesis Kit with oligo $(dT)_{18}$ primers. Real-time PCR was performed using the StepOne Real Time PCR system (Applied Biosystems). Reaction components included diluted cDNA (10ng), SYBR Green 1×, forward and reverse primer (250nM/primer). The running method for amplification and detection had the following steps: holding stage, 5 min at 95°C; 45 cycles with 20 sec at 95°C, 20 sec at 58°C, 15 sec at 72°C, 15 sec at 95°C. The data were analyzed with StepOne software v2.3. All relative quantifications (RQ) were normalized using the *Rplp1* gene expression.

RNA purification from focal adhesions

Protocol 1

To isolate FAs using the protein cross-linking protocol, cells were seeded on coated tissue culture plates. At 60-70% confluency, cells were washed three times with PBS and incubated with 3mM DTBP crosslinker in DMEM/25mM HEPES for 30 min at 37°C. DTBP was quenched by 1M Tris-HCl (pH=8) for 2 to 3 min at room temperature and cells were washed three times using ice cold PBS. Thereafter, cells were incubated with RIPA buffer (50mM Tris-HCl pH=8, 150nM NaCl, 1% Triton X-100, 0.5% SDS, 1% sodium deoxycholate, 5mM EDTA supplemented with protease inhibitors) for 15 min on ice. Cell bodies were removed by high-pressure washing with DEPC-treated ddH_2O. For RNA crosslinking, cells were UV-irradiated on ice at 100mJ/cm^2 using the UV-crosslinker BLX-254 (254nm). For proteinase K treatment, FAs were incubated with proteinase K solution for 30 min at 37°C and collected by scraping. Samples were then centrifuged at 7000rpm for 10 min at 4°C. The supernatant was discarded and RNA was isolated using Trizol.

Protocol 2

For FA isolation using a mild lysis buffer, cells were seeded on coated tissue culture plates. At 60-70% confluency, cells were washed three times with PBS, UV-irradiated and incubated with 2.5mM Triethylamine/ddH_2O (pH=7) for 10 min at room temperature. For additional crosslinking, cells were incubated with 1%PFA/PBS prior UV-irradiation (optional). Cell bodies were removed by high-pressure washing with DEPC-treated ddH_2O.

To verify FA isolation via immunofluorescence, cells were seeded on acetone-fixed, coated 13mm glass coverslips. Following FA isolation using protocol 2, coverslips were fixed in 4% PFA for 10 min at

room temperature. Thereafter, FAs were washed two times with PBS and blocked in PBS with 5% BSA for 1h at room temperature. FAs were then incubated with anti-vinculin 1 antibody in 1%BSA/PBS solution overnight at 4°C. FAs were then rinsed in PBS and incubated with Alexa Fluor 546 conjugated secondary antibody and DAPI (1:1000) for 1h at room temperature. Actin filaments were stained using Alexa 488-phalloidin (1:400). Specimens were rinsed and mounted on microscope slides using Mowiol mounting medium. Mounted FAs were analyzed by fluorescence microscopy using a Leica DFC345 FX camera and a Leica DM2000 microscope.

Trizol protocol (for RNA isolation)

For RNA extraction, FAs were incubated in Trizol reagent for 5 min at room temperature and collected by scraping. Thereafter, 0.2mL chloroform was added per 1mL Trizol reagent. After vigorous vortexing, samples were incubated for 2 to 3 min at room temperature and then centrifuged at 12000g for 15 min at 4°C. After centrifugation, samples were separated into a lower organic phase (protein, lipids), an interphase (DNA) and an upper aqueous phase (RNA). The aqueous phase was collected carefully and mixed with isopropanol (0.5mL per 1mL Trizol reagent). Samples were then incubated for 10 min at room temperature and centrifuged at 12000g for 10 min at 4°C. To visualize pelleted RNA, isopropanol-mixed samples were incubated with GlycoBlue coprecipitant for 30 min at -20°C before centrifugation (optional). The supernatant was discarded and the RNA pellet was washed with 75% ethanol (1mL per 1mL Trizol reagent), centrifuged at 7500g for 5 min at 4°C and air-dried for 5 to 10 min. The extracted RNA was dissolved in 15 to 20ul WFI and stored at -80°C. RNA quantity and quality of extracted samples were assessed with: (i) Nanodrop Spectrophotometer. (ii) Qubit 2.0 Fluorometer (Invitrogen). Each extracted RNA sample was prepared using the Qubit RNA HS (High Sensitivity) Assay kit. RNA concentration was measured using a two-standard calibration curve. (iii) Electrophoretic separation on microfabricated chips using an Agilent 2100 Bioanalyzer and the eukaryote total RNA 6000 Nano Assay kit, according to the manufacturer's instructions. Electropherograms, gel-like visualizations, RNA concentration estimations and RNA integrity number (RIN) calculations were generated for each electrophoretic trace with the 2100 Expert Software. The RIN was defined with a numbering score system from 1 (degraded) to 10 (intact).

Statistical analysis

Graphical representations were constructed in R[159] using ggplot2[160] package, unless otherwise stated. Statistical analyses were performed using the Graph Pad Prism 8. Data are presented as mean ± SEM, unless otherwise stated. Samples were compared by a non parametric Mann-Whitney U test. A value of $p \leq 0.05$ was considered as statistically significant (ns $p > 0.05$, *$p \leq 0.05$, **$p \leq 0.01$, ***$p \leq 0.001$, and ****$p \leq 0.0001$). N represents the total number of mice. Data are representative of one to three independent experiments.

3. RESULTS

3.1 Investigating the impact of PINCH on tumour-associated vasculature

To generate inducible, vascular EC-specific deletion of PINCH, we crossed mice carrying a loxP-flanked *PINCH1* gene (*PINCH*$^{fl/fl}$) to mice that express Cre recombinase under the control of an EC-specific promoter (**Fig. 8A**). Cre recombinase is fused with a mutated estrogen receptor (ER) which requires active tamoxifen (TAM) metabolites (4-OH- tamoxifen) to become activated and translocate to the nucleus, thus achieving both tissue-specific and time-dependent *PINCH1* deletion (knockout mice – hereafter referred to as KO or PINCH1 KO). Moreover, we exploited our transgenic mice by crossing with the ROSA-mTmG mouse line. ROSA-mTmG mice carry a double-fluorescent, membrane-targeted Cre reporter allele[161]. When Cre recombinase is absent or inactive, mTmG mice express red fluorescence (mTomato or mT) in a variety of cell types. After Cre recombination, the mTmG transgene is converted through the removal of the mTomato cassette and mGFP (or mG) is expressed exclusively on Cre-expressing ECs[162]. This enables us to **(i)** visualize intratumoural blood vessels and concomitantly **(ii)** monitor Cre recombinase activity (**Fig. 8B**).

To establish our *in vivo* tumour models, we performed subcutaneous inoculation of commonly used, murine cancer cell lines (B16F0 or CMT19). Mice were divided into two groups: the TAM-induced Cre-loxP experimental group and the TAM-induced group carrying the loxP-flanked *PINCH* gene without the Cre transgene (control). TAM was administered in three separate doses to achieve complete PINCH deletion in ECs. Control groups including untreated *Pdgfb-Cre*/ERT2 mice with floxed sequences and TAM-treated, wild-type mice have already been tested (data not shown) and do not present Cre leakage or TAM off-target effects, respectively.

We first evaluated the role of EC PINCH1 on tumours arising from B16F0 (melanoma) cells (**Fig. 8C**). PINCH1 deletion had no effect on tumour growth in mice with subcutaneous melanoma tumours (**Fig. 8D and 8E**). To examine properties of the tumour vascular network, we stained tumour sections for the EC-specific marker PECAM or CD31. Analysis of whole tumour sections showed no significant differences in blood vessel density (**Fig. 9A-C and Fig. 9E**). It is important to note that the blood vessel density is not proportional to the tumour volume. This means that increased tumour volume does not necessarily coincides with a high number of vessels (**Fig. SA**). Moreover, the vessel structure was similar between wild type and KO tumours (**Fig. 9D**). The same applies for the size of each individual vessel within the tumours. Despite the presence of a peak in higher vessel sizes in the case of PINCH1 KO tumours, further classification according to vessel area did not reveal significant difference (**Fig. 9F**). To address the impact of EC PINCH1 on the pericyte coverage of the tumour vasculature, we performed immunofluorescence staining to label tumour-associated vessels together with a pericyte marker (**Fig. 10A**). Further image analysis (**Fig. 10B**) indicated that the numbers of the surface area coverage were similar in control and KO tumours (**Fig. 10C and 10D**).

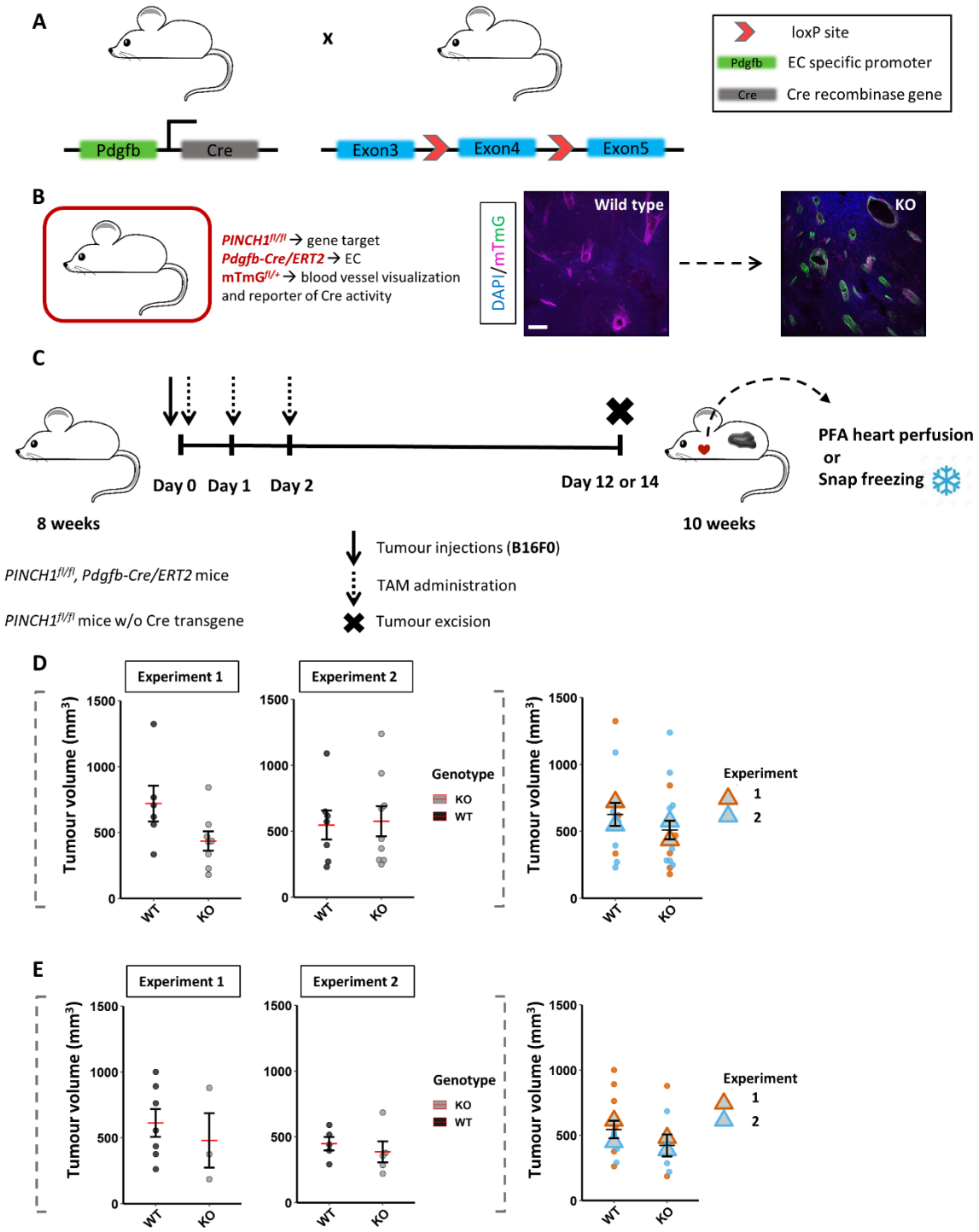

Figure 8. EC PINCH1 is dispensable for B16F0 tumour growth in adult mice. (A) Mouse breeding scheme for *PINCH1* gene targeting specifically in ECs of adult mice. Homozygous *PINCH1* floxed mice were crossed to mice carrying a *cre* transgene driven by an EC-specific promoter. **(B)** Inducible KO mice combined with the ROSA-mTmG reporter line. In wild type mice, multiple stromal cell types have red fluorescence within the tumour including immune cells, vascular cells (ECs and mural cells) and fibroblasts [163]. After EC-targeted gene KO, blood vessels are observed in green fluorescence implying efficient and specific deletion. Cell nuclei were labelled with DAPI (blue); Objective 25×; Scale bar 50um. **(C)** Experimental protocol to induce EC-specific deletion of PINCH1 in subcutaneous tumour mouse models (melanoma primary tumours). Experimental animals carried both the *PINCH1* floxed gene in the homozygous state and the Cre recombinase gene. Mice that were homozygous for *PINCH1* loxP sequences but non-carriers of the *cre* transgene were used as control. Both groups received TAM in three doses. During tumour excision (day 12 or day 14), mice were either perfused from the heart to fix the tumour tissue (used for thick section staining and confocal microscopy) or tumours were snap frozen (used for thin section tile scanning). **(D-E)** Volume quantification as described in Materials and Methods of murine tumours excised either on day 14 (D) or day 12 (E). Data from individual experiments are combined in "Superplots" for each excision timepoint. The mean from each biological replicate is represented by a colour-coded (according to experiment number) triangle.

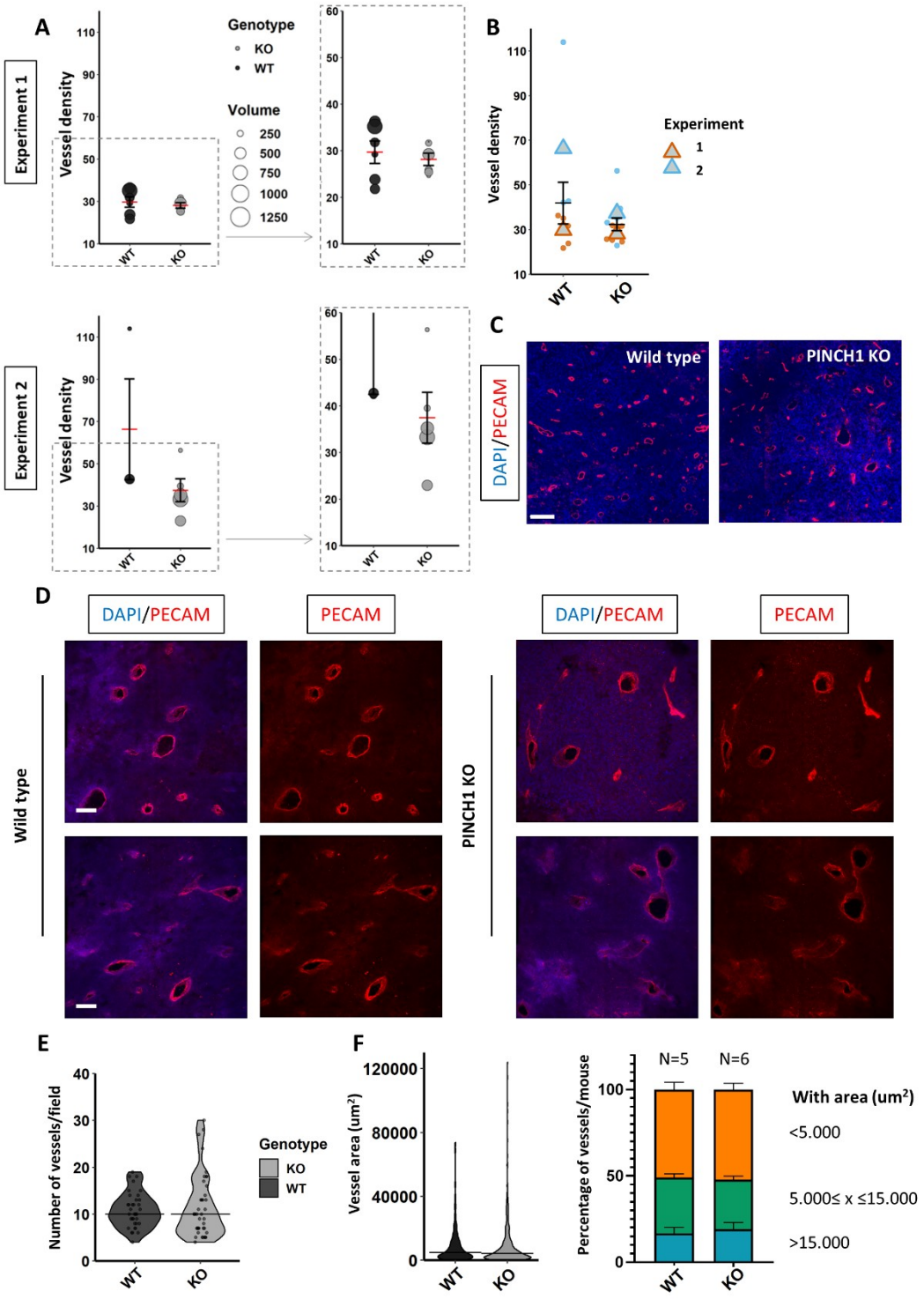

Figure 9. Ablation of PINCH1 in endothelial cells does not influence the density, structure and size of tumour-associated vessels. **(A)** Quantification of blood vessel density within B16F0 tumours (excised on day 14). The size of dots in the plot is proportional to the tumour volume of each corresponding mouse. Vessel density per section is defined as the number of vessels divided by the tumour area (mm^2). Dashed frame: focused vessel density axis. **(B)** Superplot combining the results for vessel density assessment from two independent experiments. **(C)** Representative images from tile scans that were acquired to quantify blood vessel density. Vessels were stained for PECAM (red). Cell nuclei were labelled with DAPI (blue); Scale bar 200um. **(D)** Immunofluorescence staining of thick tumour sections for PECAM (red). DAPI (blue) denotes nuclei. Images were acquired using confocal microscopy (Wild type, N=5; KO, N=5; 6-8 images per mouse); Objective 25×; Scale bar 50um. **(E)** Quantification of vessel number per microscopic field (confocal imaging), verifying the findings of blood vessel density (tile scans). **(F)** Quantification of the size of each individual vessel (confocal imaging) using the IMARIS software (6-8 images per mouse).

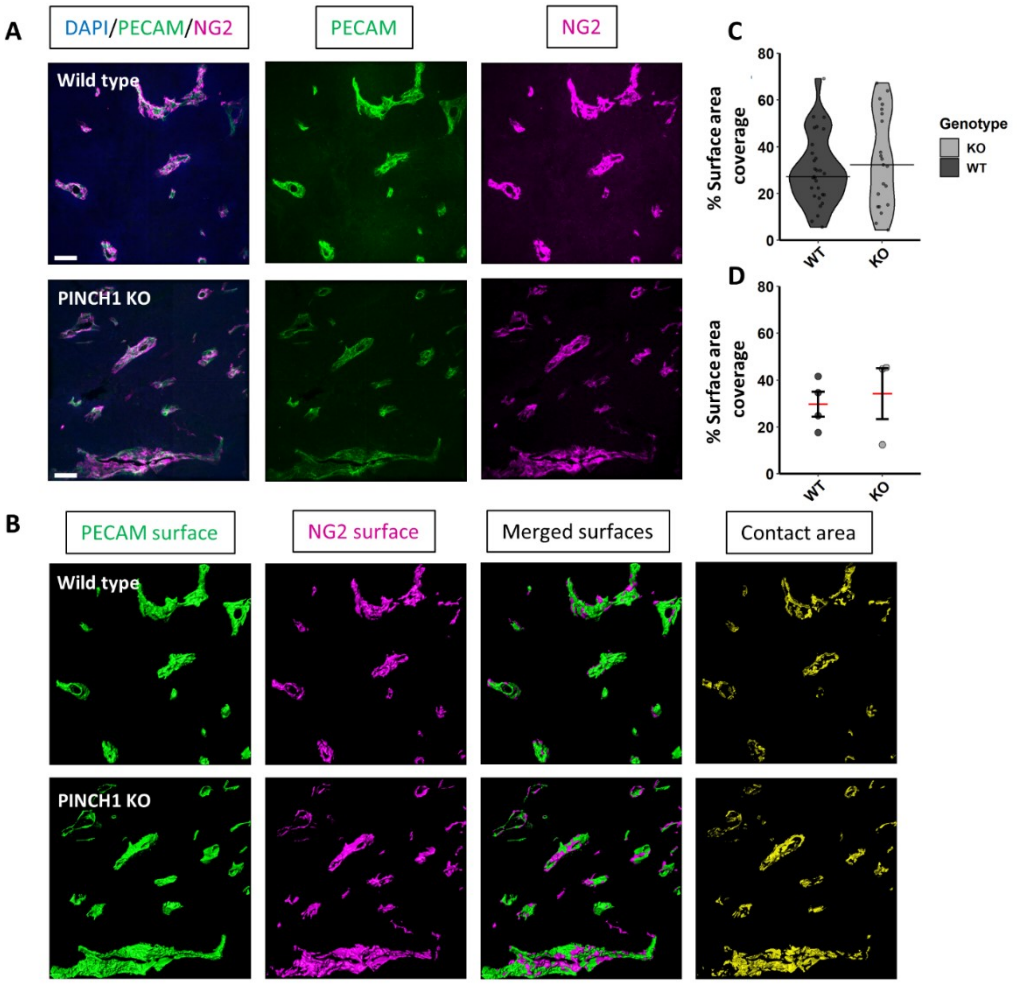

Figure 10. Conditional PINCH1 deletion in endothelial cells does not affect the pericyte coverage of the tumour vasculature. (A) Immunofluorescence staining of thick tumour sections for PECAM (green) and the pericyte marker NG2 (magenta). DAPI (blue) denotes nuclei. Images were acquired using confocal microscopy; Objective 25×; Scale bar 50um. **(B)** Image analysis using the IMARIS software. First, the surfaces of each channel were defined. Then, IMARIS calculated the area where PECAM and NG2 surfaces are attached (that is referred to as contact area). **(C)** Quantification of the surface area coverage per microscopic field (7 images per mouse). The % surface area coverage is defined as the contact area divided by the corresponding vessel area. **(D)** The averages of surface area coverage per mouse (wild type, N=4; KO, N=3).

Next, we proceeded working on subcutaneous tumour models using a different cancer cell line, named CMT19 (derived from murine lung adenocarcinoma) (**Fig. 11A**). Of note, mice with EC-specific PINCH1 deletion had a significant decrease in tumour growth compared to control littermates (**Fig. 11B**). However, the vessel number in tile scanned sections was similar between control and KO tumours (**Fig. 11C and 11D**). To examine vessel perfusion, mice were intravenously (IV) inoculated with FITC-conjugated dextran prior tumour excision. Although the numbers did not reach statistical significance, there is an obvious trend towards increased perfusion in PINCH1 KO mice (**Fig. 11D and 11E**).

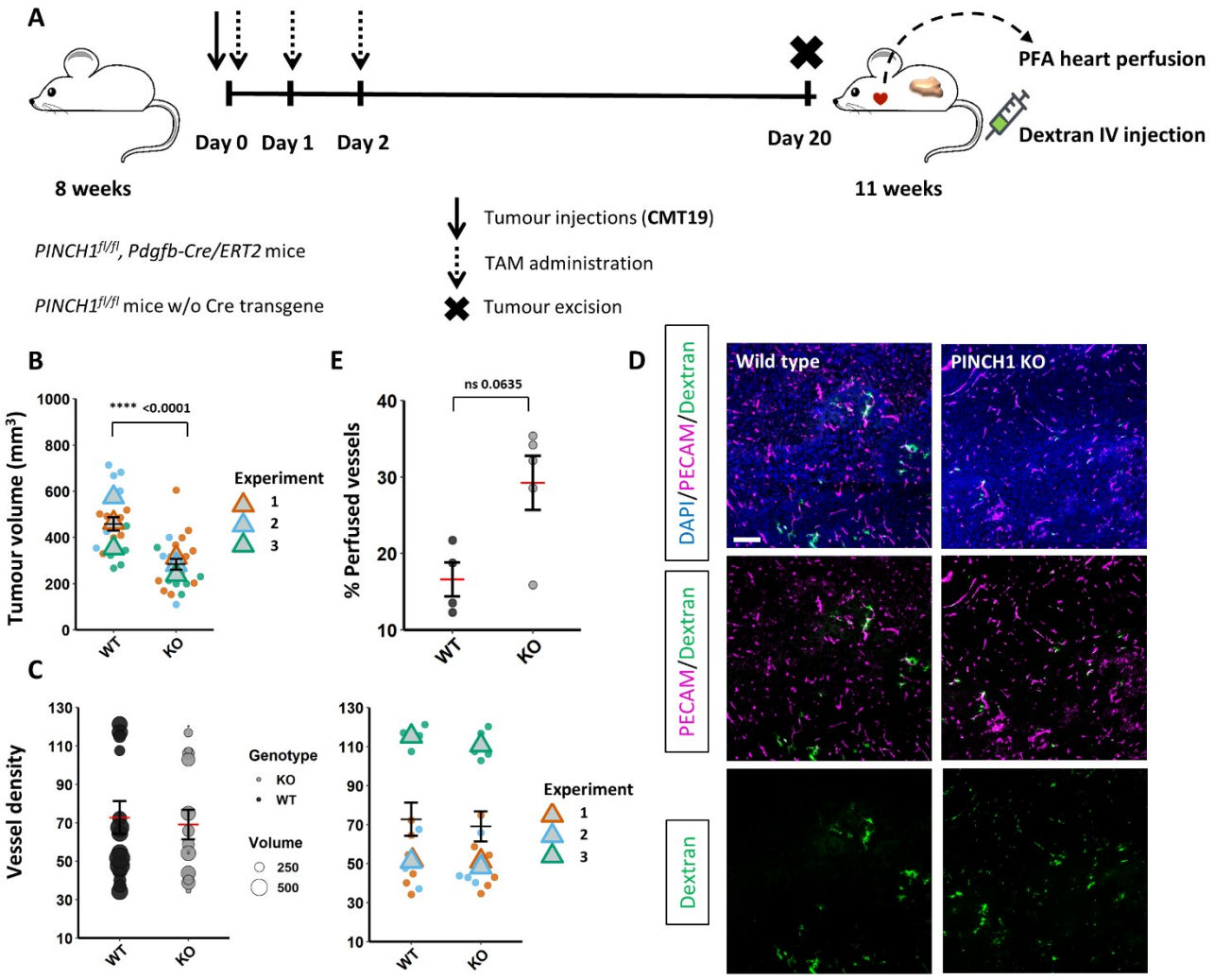

Figure 11. Ablation of PINCH1 from endothelial cells results in reduced CMT19 tumour progression *in vivo*. **(A)** Experimental protocol to induce EC-specific deletion of PINCH1 in subcutaneous tumour mouse models (lung adenocarcinoma primary tumours). During tumour excision (day 20), mice were either perfused from the heart to fix the tumour tissue (used for thick section staining and confocal microscopy) or tumours were snap frozen (used for thin section tile scanning). For vessel functionality, IV injections of FITC-dextran were given to tumour-bearing mice and excised tumours were snap frozen. **(B)** Superplot depicting CMT19 tumour volume quantification from three independent experiments. **(C)** Quantification of blood vessel density within CMT19 tumours from three independent experiments. Left: Dot plot depicting the results from vessel density assessment. The size of dots in the plot is proportional to the tumour volume of each corresponding mouse. Vessel density per section is defined as the number of vessels divided by the tumour area (mm^2). Right: Same findings presented in Superplot. **(D)** Representative images from tile scans that were acquired to quantify blood vessel density and perfusion. Vessels were stained for PECAM (magenta) and were labelled with dextran (green). Cell nuclei were labelled with DAPI (blue); Scale bar 200um. **(E)** Percentages of perfused vessels per tumour section (One experiment; Wild type, N=4; KO, N=5).

To study in detail the vessel functionality of CMT19 tumours, we observed dextran perfused sections using the confocal microscope. Image analysis showed that vessel leakage is significantly decreased in KO tumours (**Fig. 12A-C**). Moreover, tumours from PINCH1 KO mice had a significant decrease in vessel surface area measured per microscopic field (**Fig. 12B**). Statistical significance was not retained when averages for each mouse were calculated (**Fig. 12C**). To further investigate whether there is a difference in the vessel structure between wild type and KO mice, we stained tumour sections for PECAM or endomucin. The structure of vessels was also examined using the mTmG reporter transgene. The vascular network within the TME appeared to be similar in control and KO mice (**Fig. 12D**).

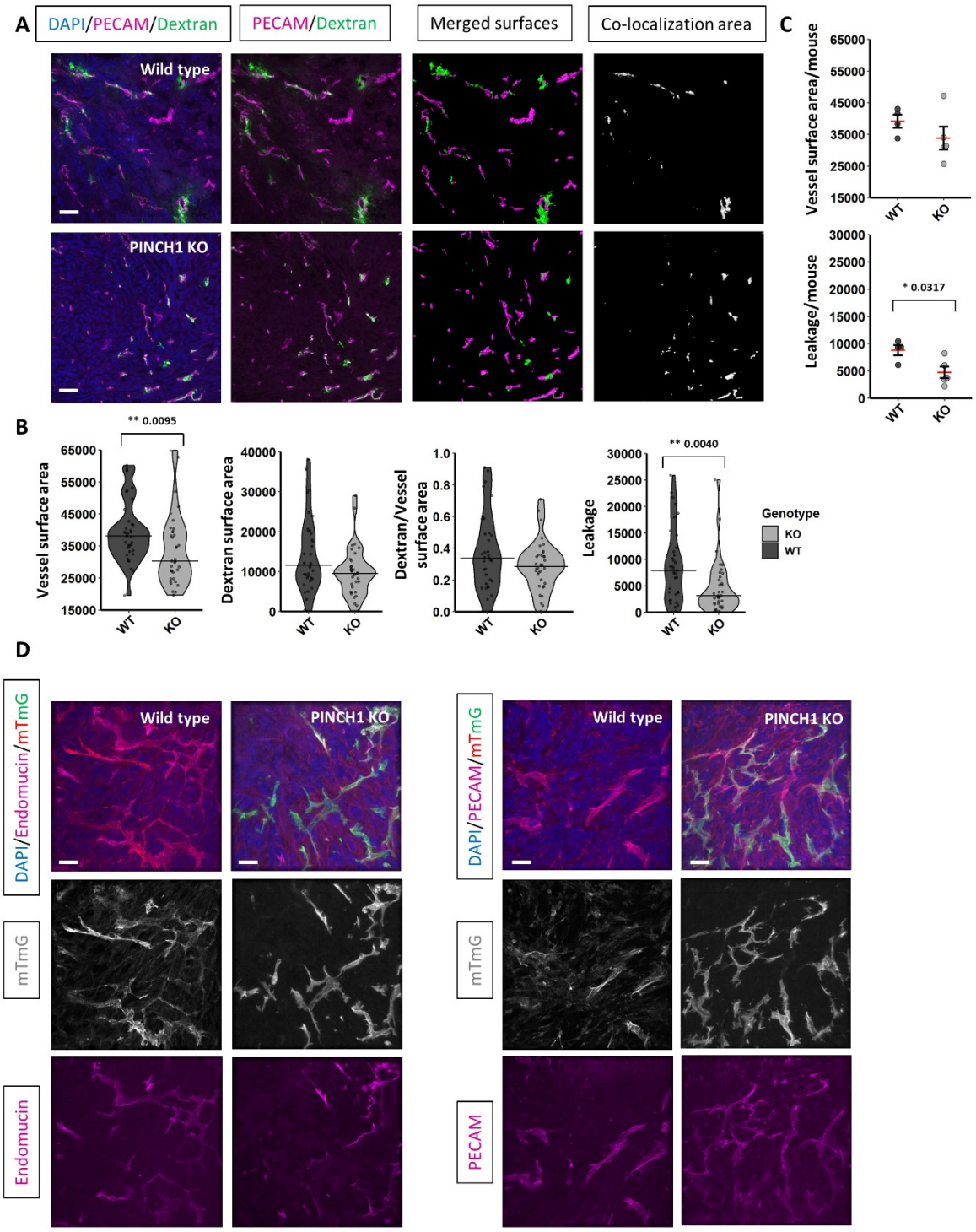

Figure 12. Deletion of EC PINCH1 decreases vessel leakage and vessel surface area within the TME of CMT19 tumour models. (A) Immunofluorescence staining of thin tumour sections for PECAM (magenta). Tumours were additionally labelled with dextran (green). DAPI (blue) denotes nuclei. Images were acquired using confocal microscopy. The surfaces of each channel were defined and the co-localization area between those surfaces was calculated using the IMARIS software; Objective 25×; Scale bar 50um. **(B)** Quantification of vessel and dextran surfaces per microscopic field (7-10 images per mouse). Microscopic fields were chosen using the PECAM channel to avoid biased acquisition. Leakage was defined by subtracting co-localization area from dextran surface area. **(C)** The averages of vessel surface area and leakage per mouse (One experiment; Wild type, N=4; KO, N=5). **(D)** Immunofluorescence staining of thin tumour sections for PECAM or endomucin (magenta). On merged images, mTmG signal is shown in red (mT) and green (mG). Single mT (wild type) or mG (KO) images for vessel visualization are shown in grey. DAPI (blue) denotes nuclei. Images were acquired using confocal microscopy (Endomucin: two experiments, 4-7 images per mouse; Wild type, N=6; KO, N=7; PECAM: two experiments, 4-6 images per mouse; Wild type, N=3; KO, N=5); Objective 25×; Scale bar 50um.

To dissect the role of EC PINCH1 in additional TME constituents, we stained with anti-alpha smooth muscle actin (aSMA) antibody and Lectin BS1 which are enriched in the tumour stroma (**Fig. 13A**). We observed a potential increase in aSMA positive ($aSMA^+$) cells in tumours grown in PINCH1 KO mice in contrast to control littermates. In higher objective magnification, we also noticed different structures in aSMA staining of KO tumours (wide and linear) compared to wild type tumours (short and spiky) (**Fig. 13A**). In addition, Lectin BS1 labelling revealed that there are conceivably reduced tumour stromal populations, including immune cells. However, the TME within subcutaneous CMT19 tumours is intrinsically fibrotic and enriched in host cells, making aSMA and Lectin BS1 stained sections unsuitable for image analysis. To overcome this caveat, we assessed:

(1) the composition of immune infiltrations in the tumour niche by CD68 and CD3 staining, a pan-macrophage marker and a T cell marker, respectively (**Fig. 13B and 13D**). A decreased presence of TAMs was found in KO tumours (**Fig. 13C**). However, the percentage of $CD68^+$ area remained unchanged in wild type and KO tile scanned tumour sections (**Fig. SB**). Moreover, no differences were observed in the average numbers of TAMs per mouse and numbers of $CD3^+$ T cells (**Fig. 13C and 13E**).

(2) the $aSMA^+$ and $vimentin^+$ cell populations by fluorescence-activated cell sorting (FACS) analysis. Tumour cell suspensions were additionally stained with anti-PECAM antibody (**Fig. 13F and SC**). We did not identify significant differences in the percentages of $vimentin^+CD31^-$, $aSMA^+CD31^-$ events, total SMA^+ or $vimentin^+$ events and ECs ($vimentin^-$ or $aSMA^-CD31^+$ events) between wild type and KO tumours (**Fig. SD-F**). The same applied for the mean fluorescence intensity (MFI) of total $aSMA^+$ or $vimentin^+$ events (**Fig. SG**). Of note, we observed a statistically significant increase in the percentages of double positive ($vimentin^+CD31^+$ and $aSMA^+CD31^+$) events in the case of PINCH1 KO tumours (**Fig. 13G**).

To investigate the effect of EC PINCH in the tumour-associated ECM composition and vessel basement membrane, tumours sections were stained for type IV collagen (collagen IV) (**Fig. SH**). Vessels were also observed using the mTmG reporter transgene or PECAM staining. We recognized an obvious decrease in collagen total abundance and less collagen on the surface of vessels of KO tumours compared to wild type tumours.

To address potential biological compensation between PINCH isoforms, we continued working on EC-specific double KO (PINCH1 and PINCH2) tumour models. We first needed to assess whether ECs, in fact, express PINCH2. For this reason, we designed novel primers targeting a PINCH2-specific carboxy-terminus (C-terminus) region (**Fig. 14A**). We confirmed expression of PINCH2 in ECs by real-time PCR on RNA from lung mouse lung ECs (MLECs) of wild type mice. RNA isolated from wild type lung non-ECs (mainly fibroblasts) was used as a positive control. Our negative control was RNA from MLECs of constitutive PINCH2 KO mice (**Fig. 14B**).

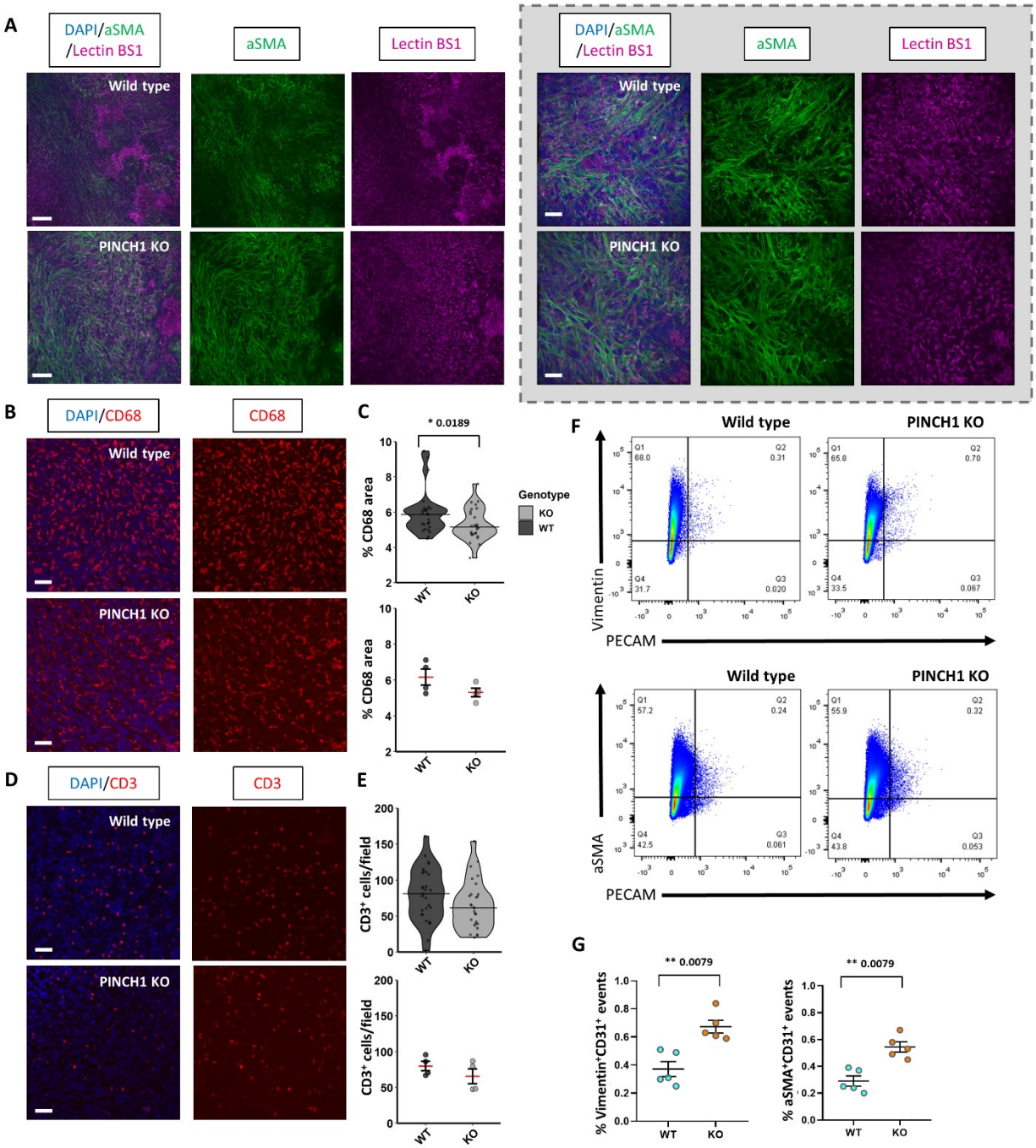

Figure 13. Ablation of EC PINCH1 alters microenvironment components of CMT19 tumours in mice. (A) Immunofluorescence staining of thick tumour sections for aSMA (green) and Lectin BS1 (magenta). Cell nuclei were labelled with DAPI (blue). Images were acquired using confocal microscopy; Left: Objective 10×; Scale bar 200 um; Right, in dashed frame: Objective 25×; Scale bar 50 um. **(B)** Representative images from thin sections stained for CD68 (red). DAPI (blue) denotes nuclei; Objective 25×; Scale bar 50um. **(C)** Percentages of $CD68^+$ area per microscopic field. Averages per mouse were also calculated (One experiment; Wild type, N=4; KO, N=4). **(D)** Representative images from thin sections stained for CD3 (red). DAPI (blue) denotes nuclei; Objective 25×; Scale bar 50um. **(E)** Quantification of $CD3^+$ cells per microscopic field. Averages per mouse were also calculated (One experiment; Wild type, N=4; KO, N=4). **(F)** Representative pseudocolour density plots of wild type and PINCH1 KO tumours. Percentages of negative, single positive and double positive cells are mentioned on the graphs. **(G)** Percentages of double positive events ($vimentin^+$ or $aSMA^+CD31^+$ events) in wild type (cyan) versus KO (orange) tumours. Graphs were constructed using GraphPad Prism 8. FACS data derive from one experiment.

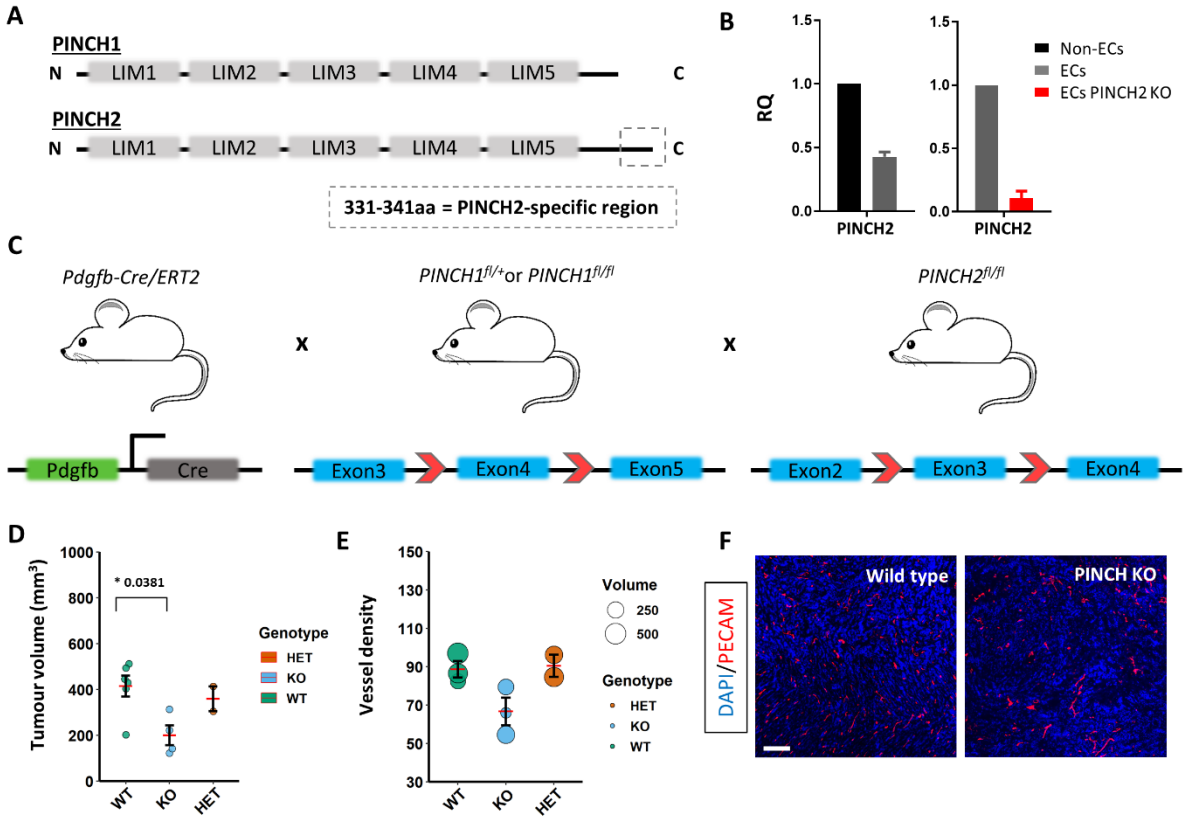

Figure 14. Complete ablation of both PINCH isoforms leads to decreased growth of CMT19 tumours. (A) Protein sequences of PINCH isoforms. PINCH2 protein carries a longer C-terminus region by ten amino acids compared to PINCH1. **(B)** *PINCH2* expression profiles of primary MLECs, non-ECs and PINCH2 KO MLECs analyzed by real-time PCR. Data are presented as mean ± SD. **(C)** Mouse breeding scheme for *PINCH1* and *PINCH2* gene targeting specifically in ECs of adult mice. Homozygous or heterozygous *PINCH1* floxed mice and homozygous *PINCH2* floxed mice were crossed to mice carrying a *cre* transgene driven by an EC-specific promoter. **(D)** Tumour volume measurements from wild type and double PINCH KO mice with subcutaneous CMT19 tumours. **(E)** Quantification of blood vessel density within CMT19 tumours. The size of dots in the plot is proportional to the tumour volume of each corresponding mouse. Vessel density per section is defined as the number of vessels divided by the tumour area (mm^2). **(F)** Representative images from tile scans that were acquired to quantify blood vessel density in wild type (left) and *PINCH1*$^{fl/fl}$*PINCH2*$^{fl/fl}$ KO (right) mice. Vessels were stained for PECAM (red). Cell nuclei were labelled with DAPI (blue); Scale bar 200um.

To induce ablation of both PINCH isoforms in ECs *in vivo*, mice that carried floxed sequences of *PINCH* genes were crossed to EC-specific Cre expressing mice (**Fig. 14C**). More specifically, we crossed mice carrying a loxP-flanked *PINCH1* gene (*PINCH1*$^{fl/fl}$) and a loxP-flanked *PINCH2* gene (*PINCH2*$^{fl/fl}$) to mice that express Cre recombinase under the control of an EC-specific promoter (KO mice). Mice that express Cre recombinase and are homozygous for the *PINCH2* floxed gene but heterozygous for the *PINCH1* floxed gene (*PINCH1*$^{fl/+}$) are referred to as HET. Mice carrying loxP-flanked *PINCH* genes without the Cre transgene were used as control.

Complete deletion of PINCH isoforms in murine CMT19 tumour models led to a significant decrease in tumour growth (**Fig. 14D**). *PINCH1*$^{fl/+}$*PINCH2*$^{fl/fl}$ KO mice (HET) showed tumour progression similar to wild type mice. Furthermore, there was an apparent decrease in the vessel density of KO tumours (**Fig. 14E and 14F**). Due to limited number of mice, this difference did not reach statistical significance. No difference was observed in the vessel number of wild type and HET mice.

3.2 Studying the local RNA translation in focal adhesions of ECs

To investigate whether RNA is localized in FAs of ECs, we performed *in vitro* experiments that combined FA isolation protocols with RNA extraction (using Trizol). To accelerate our research, we used immortalized cells spontaneously generated from primary MLECs (IMLEC). The endothelial identity of IMLEC passages used in this work was confirmed with a variety of techniques including FACS analysis (**Fig. 15A**) and immunofluorescence stainings (**Fig. 15B**) as well as cell growth analysis, real-time PCR, immunoblotting and LDL-uptake assay (data not shown).

We initially sought to extract RNA after FA isolation using an in-house, standardized protocol with a protein crosslinker and RIPA lysis (protein cross-linking protocol or protocol 1). RNA extracted from intact IMLECs was used as a positive control. RNA extraction after protocol 1 in one plate of IMLECs yielded relatively low amounts of RNA with poor purity indexes in Nanodrop (**Fig. 15C**). Consequently, we modified protocol 1 by (i) inserting a UV crosslinking step after protein crosslinking and inactivation, and (ii - optional) performing treatment with proteinase K (PK) following cell lysis and FA isolation (**Fig. 15D**).

Despite these protocol alterations and a slight increase in the number of plates used, the modified protocol 1 produced inadequate RNA extracts in terms of quantity and purity (**Fig. 15E**). Therefore, we entirely changed our FA isolation protocol by using a mild buffer (triehanolamine or TEA) for cell lysis (protocol 2) (**Fig. 15F**). Apart from UV-induced crosslinking, crosslinking with paraformaldehyde (1% PFA) was performed (optional). We confirmed with immunofluorescence staining that protocol 2 efficiently isolated FAs both from IMLECs and primary MLECs (**Fig. 15G**). Comparison of protocol 2 with 1% PFA treatment or mild lysis only (TEA only) revealed that more remaining nuclei were obtained in the first case. To avoid nuclear contamination, we performed RNA extraction from seven plates of IMLEC FAs isolated with protocol 2 (TEA only). Nanodrop quantitation showed low purity ratios. However, we run this RNA extraction sample using two additional technologies (Qubit and Bioanalyzer). Qubit managed to detect 18.2 ng/ul of RNA (**Fig. 15E**). Furthermore, this RNA extract exhibited high RIN score (8.6) and RNA concentration equal to 7 ng/ul (**Fig. 15I**).

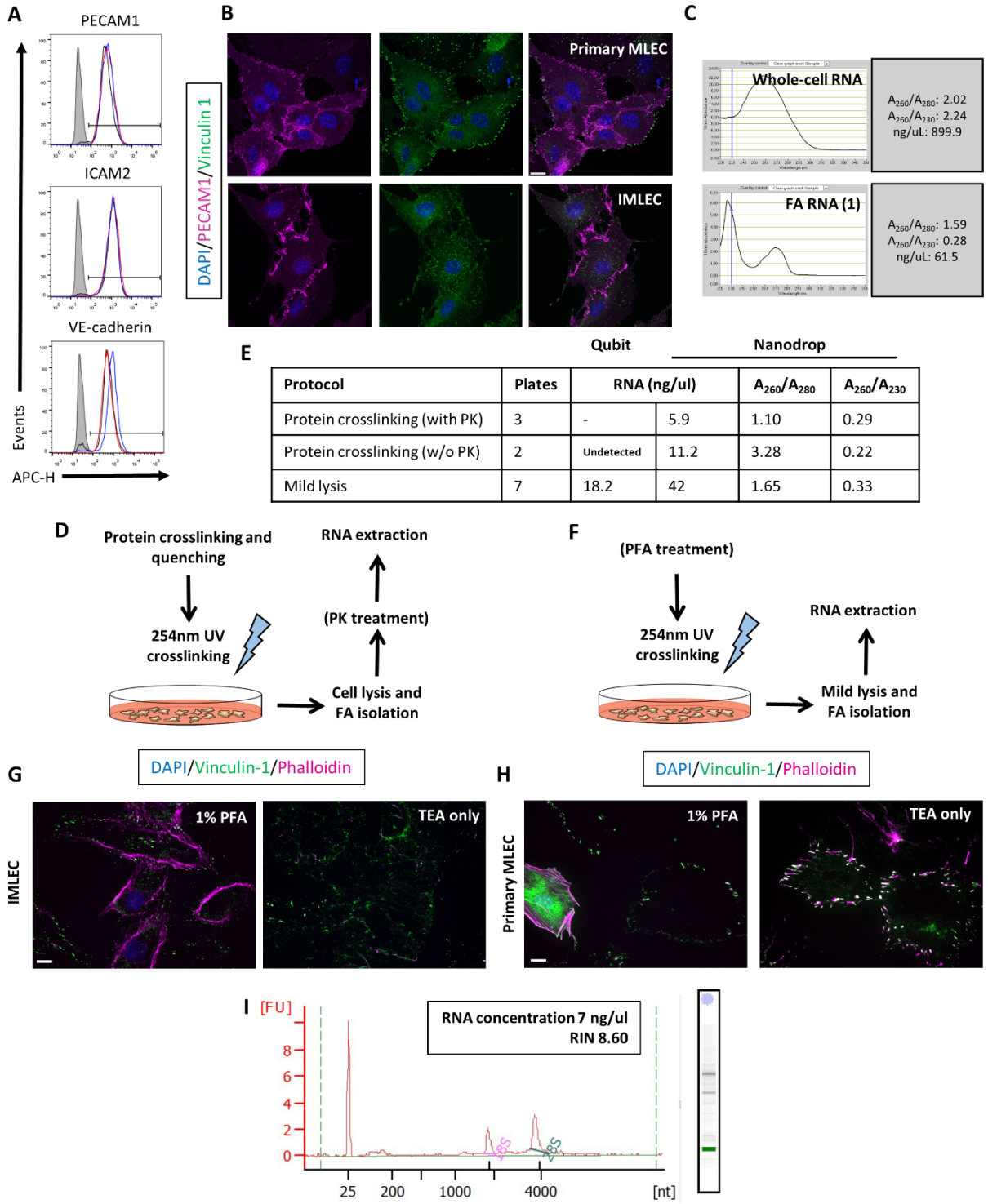

Figure 15. Investigating the presence of RNA in EC focal adhesions. (A) FACS analysis of primary (black) and immortalized (red and blue) MLECs for surface endothelial markers. Grey histograms depict unstained, negative control samples. **(B)** Immunofluorescence staining of primary MLECs and IMLECs for PECAM1 (magenta) and vinculin 1 (green). Cell nuclei were stained with DAPI (blue). Scale bar 20µm. **(C)** Nanodrop measurements of RNA isolated from IMLEC FAs using the protein crosslinking protocol without modifications (protocol 1). The RNA concentration and purity ratios are mentioned in black-bordered frames. **(D)** Modified protocol 1 for FA isolation. Optional steps are enclosed in parenthesis. **(E)** Table of RNA extractions using alternative FA isolation protocols (modified protocol 1 and protocol 2). **(F)** Mild lysis protocol for FA isolation (protocol 2). Optional steps are enclosed in parenthesis. **(G-H)** Immunofluorescence staining with anti-vinculin 1 antibody (green) of FAs isolated following the mild lysis protocol with (1% PFA) or without (TEA only) PFA from IMLECs **(G)** and primary ECs **(H)**. Cytoplasmic residues were labelled with phalloidin (magenta). Cell nuclei were stained with DAPI (blue). Scale bar 20µm. **(I)** Bioanalyzer run of RNA extracted from seven plates of IMLEC FAs using the mild lysis protocol (TEA only). Electropherogram (peaks) and gel-like image (bands) show from left-to-right and down-to-up direction, respectively: the pre-region marker, the 18S fragment, the 28S fragment. The RNA concentration and RIN are mentioned in a black-bordered frame.

4. DISCUSSION

Integrin signalling is intimately implicated in various aspects of cell behaviour and motility, regulating fundamental processes including cell division, the assembly of actin-cytoskeleton and cell survival[126]. Consequently, integrin signalling has been characterized as a key player in the initiation and progression of solid tumours influencing both malignant (for example proliferation, invasion and migration[150]) and tumour-associated host cell states (vascular endothelium role in angiogenesis[100])[96]. PINCH is a main mediator of integrin-related signalling that functions as an adaptor protein forming molecular hubs for signal transduction[137]. Despite current evidence identifying PINCH-interacting partners, their roles and association with human diseases[149], our understanding of PINCH function in tumour-associated vascular biology remains elusive.

In this thesis, we investigated the impact of EC-specific PINCH1 deletion *in vivo* on two distinct tumour models (subcutaneous inoculation of either B16F0 or CMT19 cancer cells) following three methodologies: **(1)** Assessment of tumour growth, **(2)** investigation of intrinsic properties of tumour vasculature and **(3)** evaluation of additional TME constituents. Deletion of the *PINCH1* gene in murine embryos leads to early lethality due to defects in egg cylinder formation, decreased cell proliferation and excessive cell death[129]. Constitutive loss of PINCH1 specifically from ECs is also embryonic lethal (E15.5) due to haemorrhaging and edema (Arapatzi and Kostourou, unpublished data), implying that PINCH1 acts as an important mediator of EC function. To avoid the difficulties associated with embryonic lethality, we used conditional KO mice generated with the tamoxifen-inducible Cre/loxP system (CreERT). Exploiting the *Pdgfb* gene promoter for the expression of EC Cre-recombinase, we were able to investigate PINCH role in a spatiotemporal manner.

B16F0 tumour growth was not affected after EC-specific PINCH1 deletion in mice. Loss of PINCH1 did not impact vessel number, structure and size. In addition, we observed no difference in the pericyte coverage of tumour vessels between wild type and KO tumours. On the contrary, tumours deriving from CMT19 injections showed a significant decrease in growth due to loss of PINCH1 in ECs. In addition, blood vessels within the tumour niche of KO mice were more functional (less leaky and more perfused). The findings for vessel functionality derive from one individual experiment. Experiment repeats and increase in the number of mice can potentially unravel a statistically significant difference for KO perfused vessels. Moreover, vessel perfusion can be studied via PE-PECAM antibody (instead of FITC dextran) IV injections. Apart from a significant decrease in the vessel surface per microscopic field of KO tumour vessels, no alterations in blood vessel density or structure were detected.

Based on recent findings in the lab, EC specific deletion of ILK decreases tumour growth and tumour angiogenesis (reduced vessel density) in both B16F0 and CMT19 subcutaneous models. Loss of ILK from ECs leads to structural abnormalities (blocked lumens) of the tumour vasculature (Arapatzi and Kostourou, unpublished data). These data indicate that members of the ternary IPP complex may have

individual, rather than/in addition to synergistic, functions in tumour-associated ECs. Nevertheless, a detailed examination of double PINCH KO mice (deletion of both isoforms) is needed to ensure that PINCH loss does not cause alterations in tumour vessel properties that phenocopy ILK loss.

PINCH1 deletion showed distinct responses in B16F0 versus CMT19 tumours in terms of tumour progression and vessel functionality. CMT19 tumours are intrinsically more fibrotic and rich in host cells compared to B16F0 tumours. We therefore explored whether this phenotypic difference is driven by a crosstalk of ECs with other TME cell types. Although we defined an increase in aSMA positive tumour stroma, our observations were not consistent with FACS results. We also noticed that aSMA stained tumour sections contain different structures (WT: wide and linear, KO: short and spiky), implying PINCH1-mediated alterations in ECM composition and abundance. We observed a decrease in collagen IV levels within the tumour stroma and in association with tumour blood vessels. However, these findings are preliminary and we need to examine and analyze more size-matched tumours of wild type and KO mice. Additional approached that could be used to study tumour fibrosis and ECM (in particular collagen) structures are second-harmonic generation microscopy[164] and immunohistochemical analysis (Picrosirius red staining)[165]. Of note, we identified a significant increase in $aSMA^+$ or $vimentin^+$ and $CD31^+$ cells within PINCH1 KO tumours, suggesting that PINCH regulates endothelial to mesenchymal transition (EndoMT) within the tumour niche. These findings are contradictory to a recent study showing that ECs undergo EndoMT in an ILK-induced manner *in vitro*[166]. Even so, experimental repeat and a comprehensive investigation (expression of additional endothelial -CD144 and claudin- versus mesenchymal markers -FSP1 and N cadherin-, *in vitro* approaches) are required to ensure that ECs are converted to CAF-like cells.

In addition, we investigated the impact of PINCH1 depletion on immune cells infiltrating CMT19 tumours. Although there was a significant decrease of macrophage presence per microscopic field in KO tumours, no differences in macrophage and T cell recruitment was observed. To verify our results and further investigate immune TME, a multi-colour FACS experiment targeting a variety of cell types should be applied (for instance: CD45: immune cells; CD11b, Gr-1 and Siglec-F: monocytic and polymorphonuclear innate populations; F4/80: macrophages; CD3, CD4 and CD8: T cell populations; B220 or CD19: B cells).

The absence of a phenotype (B16F0) or the presence of a "mild" phenotype (CMT19) in PINCH1 KO tumours may signify redundancy between PINCH isoforms on murine endothelium. Of note, EC loss of PINCH2 does not impact CMT19 tumour growth or tumour vessel number and perfusion (Arapatzi and Kostourou, unpublished data). PINCH1 was previously found to be expressed in MLECs (immortalized through retroviral induction)[167]. To test whether PINCH isoforms functionally compensate for each other, we verified PINCH2 in primary MLECs and generated KO mice combining EC-specific PINCH1 and PINCH2 loss-of-function. We used CMT19 cancer cells to induce subcutaneous tumours because we recognized a PINCH1-mediated effect with this tumour model. Double KO tumours had decreased growth, verifying our findings in single PINCH1 deletion. Interestingly, tumour vessel number appeared

to decrease in double KO mice and can possibly reach statistical significance after experimental repeat. To examine if PINCH1 controls tumour vasculature in a dose-dependent manner, we also studied tumour-bearing KO mice heterozygous for PINCH1 floxed alleles and homozygous for PINCH2 floxed alleles (HET). HET mice showed tumour progression and tumour vessel density similar to wild type mice when either CMT19 or B16F0 (data not shown) cancer cells were used.

In contrast to PINCH1, mice with constitutive, either total or EC specific depletion of PINCH2 are viable and fertile, with no evident phenotype[132] (Arapatzi and Kostourou, unpublished data). Together with our *in vivo* data, these findings suggest that PINCH isoforms are not fully redundant. This premise is also supported by the fact that **(i)** only PINCH1 interacts with RSU-1, **(ii)** PINCH isoforms are differentially expressed during development[133], **(iii)** PINCH2 overexpression in PINCH1-depleted cells restores IPP assembly but does not functionally compensate for PINCH1 loss-of-function phenotype (increased apoptosis and decreased cell spreading) *in vitro*[135] and **(iv)** unlike PINCH1, PINCH2 expression has been found to decrease in cancer cell lines promoting cell migration[149].

Many lines of investigation implicate the IPP members ILK and parvin in endothelial function. ILK deletion exclusively on murine ECs *in vivo* using the Cre/loxP system (EC-specific promoter Tie2) caused delayed embryonic development (E9.5) and demise (E11.5-12.5) due to placental vascular abnormalities[147]. Mechanistically, ILK loss was associated with defective integrin-matrix adhesion, actin cytoskeleton re-arrangements, decreased β1 integrin activation, decreased Akt phosphorylation and increased apoptosis in mouse ECs[147]. However, the impact of ILK in EC survival was proved to be Akt-independent[147]. *In vitro* experiments in bovine aortic ECs (ILK knockdown via RNA interference) showed that ILK is essential for fibrillar adhesion assembly, cell spreading, migration and tube formation[168]. In a separate study using embryoid bodies, ILK deficiency in ES cells attenuated vessel-like structure development[169]. This notable effect was attributed to impaired response to VEGF and epidermal growth factor (EGF) due to defective formation of caveolae (a type of lipid raft enriched in ECs responsible for molecular clustering and signal transduction)[169]. In particular, the localization of caveolin-1 (a core component of caveolae) in the plasma membrane was diminished and the organization of actin and microtubule cytoskeleton was perturbed[169]. A recent study also suggested that EC-specific lack of ILK in postnatal mice severely disrupts retinal (decreased vascular development, number and branching) and brain angiogenesis[146]. Abnormal sprouts with dense clusters of ECs, irregular endothelial cell-cell contacts, increased retinal recruitment of F4/80-positive macrophages and decreased EC proliferation were also reported within murine KO retinas[146]. Concomitantly, administration of ILK inhibitors in murine tumour models (glioblastoma, prostate cancer and melanoma xenografts) retards tumour growth and mediates anti-angiogenic effects (decrease tumour-associated vessel density and perfusion and increase tumour EC apoptosis)[170–172]. It was further shown that ILK promotes VEGF-driven EC migration, proliferation and angiogenesis *in vitro* and *in vivo*[172,173]. Despite a decrease in tumour progression, ILK inhibition in an orthotopic xenograft model of pancreatic cancer did not result in decreased vessel number and area within the TME[174].

As for α-parvin (the most studied parvin isoform), constitutive inactivation in ECs leads to late (E14.5) embryonic lethality owing to haemorrhaging, vessel tortuosity and decreased vessel density[148]. Interestingly, deletion of α-parvin in postnatal ECs phenocopies ILK KO retinas[146,148]. *In vitro*, α-parvin is critical for cell migration, VE-cadherin contact stability, assembly of focal complexes and actin cytoskeleton arrangement in human umbilical vein ECs (HUVECs)[148]. It is important to mention that deletion of α- and β- parvin in ECs is embryonic lethal at earlier timepoint (E10.5-E12.5) and causes additional vascular defects (such as impaired pericyte coverage) compared to single KO embryos[148,175]. Double KO mice (EC-specific α-parvin$^{fl/+}$, β-parvin$^{-/-}$) had normal embryonic development[175]. Collectively, these findings partially agree with our work and provide valuable information about potential effects of PINCH on normal and tumour angiogenesis in an IPP-dependent manner.

Nevertheless, focusing specifically on PINCH, there are lines of evidence suggesting the presence of IPP-independent activities either within or outside IACs. For instance, apart from RSU-1, PINCH1 forms distinct interaction with Nck-2 via LIM4 domain. Nck-2 is linked to growth factor signalling components (including PDGFR and EGFR[176]) and mediators of actin polymerization[177], wiring integrin adhesions with growth factor signalling and cytoskeleton assembly. Furthermore, it was recently found from Karaköse et al. (2015) that PINCH1 deletion in keratinocytes leads to more severe defects in adhesion, cell shape and migration compared to ILK deletion. In the same study, the authors identified that **(i)** in the absence of ILK, a small fraction of PINCH1 is localized within FAs and **(ii)** ELPIN is a novel interacting partner of PINCH which may contribute to actin dynamics and FA signalling[141]. Moreover, PINCH is mainly identified in IACs but nuclear localization has also been reported[120,178]. Indeed, both PINCH isoforms contain nuclear localization signals in the C-terminus region but the potential nuclear function of PINCH remains unknown.

Overall, this project was focused on the role of PINCH1 on endothelium under a tumour concept. Using subcutaneous tumour models and inducible genetic tools that target ECs, we showed that PINCH1 is necessary for tumour-promoting vascular function in a context-dependent manner. Moreover, PINCH1 and PINCH2 deletion seems to recapitulate the phenotype observed in single PINCH1 deletion and is likely to cause greater changes in the tumour vasculature. Future investigations should draw attention to:

(i) The detailed role of PINCH1 deletion in CMT19 subcutaneous tumours and other tumour types (Lewis lung carcinoma or LLC). The phenotype of PINCH loss is currently reminiscent to "vessel normalization" (such as decreased leakage, no striking effect in vessel structure). For example, it would be interesting to compare hypoxia levels (using pimonidazole adducts[179]) or response to chemotherapy of PINCH1 KO and wild tumours.

(ii) What renders CMT19 tumours "responsive" to PINCH1 deletion compared to B16F0 tumours. Significant alterations that are crucial for tumour progression should not occur in B16F0 tumours.

(iii) The effects of inactivation of both PINCH isoforms in our experimental setup (tumour growth – tumour vasculature – TME components).

(iv) The underlying molecular mechanisms that are related to PINCH deficiency on endothelial cells through further *in vitro* experiments (including cell survival assessment, investigation of FA proteins and signalling pathways).

The second aim of this thesis was to investigate whether local RNA translation occurs in FAs of ECs. Proteomics analysis of endothelial adhesome in our lab revealed the presence of RNA-binding proteins or RBPs (Rouni and Kostourou, unpublished data). To assess whether RNA is also localized in endothelial FAs, we initially sought to extract RNA from FAs isolated with an in-house, protein cross-linking protocol (protocol 1) from IMLECs. Protocol 1 failed to yield significant amounts of high-quality RNA. Therefore, we applied the following modifications: **(i)** UV-crosslinking. It induces the formation of covalent bonds between direct RNA-protein interactions[180]. **(ii)** Treatment with PK to ensure that RNA is not "trapped" within the organic phase due to UV-crosslinking[181]. **(iii)** Increase in the number of tissue culture plates used. However, protocol modifications did not increase the concentration or improved the quality of extracted RNA. We hypothesized that RNA is destroyed during lysis due to the high stringency conditions of RIPA buffer. Therefore, we standardized a protocol using mild lysis (protocol 2) for FA isolation. The efficacy of protocol 2 was confirmed via immunofluorescence for vinculin 1-stained focal adhesions and phalloidin-labelled filamentous actin. Using protocol 2, we managed to extract sufficient amounts of RNA in terms of quantity and quality.

A growing body of evidence suggests that RNA and RBPs are present to support translation within IACs. For example, the presence of actin mRNA in lamellipodia has been reported in fibroblasts, potentially facilitating rapid translation in sites of function[182]. De Hoog and colleagues (2004) performed immunoprecipitation against talin, paxillin or vinculin combined with mass spectrometry and identified cell-matrix adhesion-dependent RBPs. The authors defined fibroblast-specific, intracellular structures formed during initial cell spreading (termed as spreading initiation centres or SICs)[183]. SICs were composed of an RBP-rich core surrounded by an actin sheath and were positive for FA markers[183]. Moreover, they showed that ribosomal RNA is localized in SICs using nucleic acid fluorophores (SYTOX), RNase treatment and *in situ* hybridization assays[183]. This study provided initial leads regarding the role of RNA in cell adhesion. Of note, the structural features of interaction between vinculin and an RBP named raver1 were deciphered, implying that this interaction acts as a link for mRNA localization to IACs[184]. The impact of the RBP Polypyrimidine tract binding protein (PTB) on FA assembly and vinculin mRNA recruitment in FAs was also shown by Babic et al. (2009)[185]. Furthermore, ribosomes, translation regulators and RBPs were found to localize in focal complexes of fibroblasts[186].

Although our work shows that RNA is present within endothelial FAs, we acknowledge limitations in our study. First, the common approach among extraction trials for RNA quality control was Nanodrop

measurements. Nanodrop instruments are not sensitive in detecting small amounts of RNA compared to Qubit and Bioanalyzer technologies. Therefore, we cannot exclude the possibility of having sufficient, high-quality RNA from protocol 1 methodologies where Qubit and Bioanalyzer were not used. Second, we performed a scale-up from two to seven plates of FAs, without testing intermediate numbers. Third, possible contamination from cytoplasmic residues cannot be assessed at this point. We used the TEA only protocol to limit nuclear and cytoplasmic contamination as much as possible. Challenges accompany FA isolation due to low-affinity interactions (this is partly resolved using protein cross-linkers) and the dynamic nature of IACs (for example, RNA translation is likely to occur in early IAC assembly[115])[187]. Future experiments should focus on workflow standardization (such as the selection of FA isolation protocol after appropriate RNA quality control and the use of a viable number of tissue culture plates), the identification of appropriate negative controls and application on primary MLECs. The hypothesis of RNA presence within endothelial FAs may be augmented by immunoprecipitation experiments against adhesome-related RBPs, *in situ* hybridization assays and live-cell RNA monitoring[188]. This project is likely to pave the way to determine the endothelial FA-associated transcriptome and the effects of adhesion proteins in FA-mediated translation of ECs.

5. SUPPLEMENTAL MATERIAL

Antibodies

Antigen	Host	Vendor	Identifier	Dilution
aSMA	Mouse	Sigma-Aldrich	A2547; RRID:AB_476701	1:400 (FACS)
aSMA FITC	Mouse	Sigma-Aldrich	F3777; RRID:AB_476977	1:400 (IF)
Collagen IV	Rabbit	Bio-Rad	2150-1470; RRID:AB_2082660	1:250 (IF)
ICAM2 (CD102)	Rat	BD Biosciences	553326; RRID:AB_394784	1:500 (FACS)
CD3 Alexa Fluor 594	Rat	BioLegend	100240; RRID:AB_2563427	1:500 (IF)
CD68	Rat	Abcam	ab53444; RRID:AB_869007	1:100 (IF)
VE-cadherin Alexa Fluor 647	Rat	BD Biosciences	562242; RRID:AB_2737608	1:100 (FACS)
Vimentin	Mouse	Sigma-Aldrich	V2258; RRID:AB_261856	1:400 (FACS)
Vinculin 1	Mouse	Sigma-Aldrich	V9264; RRID:AB_10603627	1:400 (IF)
NG2	Rabbit	Millipore	AB5320; RRID:AB_91789	1:200 (IF)
PECAM-1	Rat	BD Biosciences	553370; RRID:AB_394816	1:250 (IF) 1:200 (FACS)
PECAM-1 Alexa Fluor 488	Goat	R and D Systems	FAB3628G; RRID:AB_10972784	1:200 (FACS)
Mouse IgG Cy5	N/A	N/A	N/A	1:500 (FACS)
Mouse IgG CF488A	Donkey	Biotium	20014; RRID:AB_10561327	1:400 (IF)
Mouse IgG Alexa Fluor 546	Goat	Thermo Fisher Scientific	A-11003; RRID:AB_2534071	1:400 (IF)
Rabbit IgG Alexa Fluor 488	Donkey	Thermo Fisher Scientific	A-21206; RRID:AB_2535792	1:400 (IF)
Rabbit IgG Dylight 649	Goat	Thermo Fisher Scientific	35565; RRID:AB_614945	1:400 (IF)
Rat IgG Alexa Fluor 546	Goat	Thermo Fisher Scientific	A-11081; RRID:AB_2534125	1:400 (IF)
Rat IgG Alexa Fluor 555	Goat	Thermo Fisher Scientific	A-21434; RRID: AB_2535855	1:400 (IF)
Rat IgG Alexa Fluor 633	Goat	Thermo Fisher Scientific	A-21094; RRID:AB_2535749	1:400 (IF) 1:400 (FACS)

Abbreviations: FACS, Flow cytometry analysis; IF, Immunofluorescence.

Assay kits

Resource	Vendor	Identifier
Eukaryote total RNA 6000 Nano Assay Kit	Agilent Technologies	5067-1511
FIX & PERM Cell Permeabilization Kit	Thermo Fisher Scientific	GAS004
Qubit RNA HS (High Sensitivity) Assay Kit	Invitrogen	Q32855
RNeasy Mini Kit	QIAGEN	74104
RevertAid First Strand cDNA Synthesis Kit	Thermo Fisher Scientific	K1621
SuperScript III First Strand cDNA Synthesis Kit	Thermo Fisher Scientific	18080

Chemicals

Reagent	**Vendor**	**Identifier**
Tamoxifen	Cayman Chemical	12358
Paraformaldehyde	Alfa Aesar	A11313
FITC-Dextran	Sigma-Aldrich	60842-46-8
Sucrose	Thermo Fisher Scientific	10645312
Tris Base	Thermo Fisher Scientific	10376743
HCl	Themo Fisher Scientific	10294190
EDTA	Themo Fisher Scientific	6381-92-6
Proteinase K	Sigma-Aldrich	BP1700
NaCl	Sigma-Aldrich	7647-14-5
Sodium Lauryl Sulfate	Thermo Fisher Scientific	BP166-500
Isopropanol	Thermo Fisher Scientific	BP26181
Ethanol absolute	VWR Chemical	64-17-5
KCl	Sigma-Aldrich	P5405
$MgCl_2$	AppliChem	A4425
NP-40	N/A	N/A
dNTPs	Thermo Fisher Scientific	R0181
Taq enzyme	Homemade	N/A
Bromophenol blue	Merck Millipore	115-39-9
Xylene cyanol	N/A	N/A
Glycerol	Sigma-Aldrich	G-5150
Agarose	Thermo Fisher Scientific	BP160-500
Acetic acid glacial	Thermo Fisher Scientific	10394970
Ethidium bromide	Sigma-Aldrich	E-7637
Killik OCT	Bio-Optica	05-9801
Ham's F-12	Biosera	LM-H1235
Dulbecco's Modified Eagle's Medium Low Glucose	Sigma-Aldrich	D6046
Dulbecco's Modified Eagle's Medium High Glucose	Gibco	41966
Penicillin-Streptomycin	Biosera	XC-A4122
Glutamine stable	Biosera	XC-T1755
Heparin	Sigma-Aldrich	H3149
Fetal Bovine Serum	Biosera	FB-1001
Endothelial Cell Growth Supplement	Corning	356006
GlutaMAX	Gibco	35050
Gelatin	Sigma-Aldrich	G2500
Collagen Type I	Merck Millipore	08-115
Fibronectin	Sigma-Aldrich	F0556
Trypsin	Biowest	L0930
Dulbecco's Phosphate-Buffered Saline	Gibco	14200-067
DMSO	Sigma-Aldrich	D8418
Trypan Blue	Sigma-Aldrich	T8154
Triton-X-100	Thermo Fisher Scientific	BP151
BSA	Sigma-Aldrich	A9647
Alexa 488-phalloidin	Thermo Fisher Scientific	A12379
Lectin from *Bandeiraea simplicifolia* (*Griffonia simplicifolia*) TRITC	Sigma-Aldrich	L5264
DABCO	Sigma-Aldrich	D2522
Mowiol 4-88	Merck Millipore	475904
cOmplete ULTRA Tablets, EDTA-free, EASYpack Protease Inhibitor Cocktail	Sigma-Aldrich	05892791001
Acetone	Thermo Fisher Scientific	10162180
DTBP	Thermo Fisher Scientific	20665
HEPES	Sigma-Aldrich	H7523
Sodium deoxycholate	Sigma-Aldrich	D6750
Triethylamine	Sigma-Aldrich	T9534

TRI Reagent solution	Thermo Fisher Scientific	AM9738
Chloroform	Sigma-Aldrich	C2432
GlycoBlue coprecipitant	Thermo Fisher Scientific	AM9516
SYBR Select Master Mix	Thermo Fisher Scientific	4472920

Primers

Resource	**Identifier**
PDGF F	5'- GCC GCC GGG ATC ACT CTC G -3'
PDGF R	5'- CCA GCC GCC GTC GCA ACT C -3'
mTmG F	5'- CTC TGC TGC CTC CTG GCT TCT -3'
mTmG R1	5'- CGA GGC GGA TCA CAA GCA ATA -3'
mTmG R2	5'- TCA ATG GGC GGG GGT CGT T -3'
PINCH1 F	5'- CTA GGC TGG TAA TGC AGG CC- 3'
PINCH1 R1	5'- CCT GCC AAT GAT GAA TTC AC -3'
PINCH1 R2	5'- CGC AGT TGG CAC AGT TGA AG -3'
PINCH2 F	5'- CAC TCC CAA TTC CCC TCC CTG AG -3'
PINCH2 R	5'- AGG GGT CTG AGG TCC TGA GAA GG -3'
Rplp1 F (qRT-PCR)	5'- GTG GAG GCA AAG AAG GAA GA -3'
Rplp1 R (qRT-PCR)	5'- TCA GCT CTT TAT TAG CCA ACT TAA C -3'
PINCH2 F (qRT-PCR)	5'- AAG CTG TCC GAC CTG AGC TC -3'
PINCH2 R (qRT-PCR)	5'- CAG AAG TGG GAG GTG GCT AG -3'

Cell lines

Resource	**Vendor**	**Identifier**
Mouse melanoma B16F0 (C57BL/6J)	ATCC	CRL-6322
Mouse lung adenocarcinoma CMT19	ATCC	N/A

Software

Resource	**Vendor**	**Identifier**
2100 Expert Software	Agilent Technologies	https://www.agilent.com/
ImageJ	National Institute of Health	https://www.imagej.net
IMARIS 8.2.1	Bitplane	https://www.bitplane.com
Prism 8	GraphPad	https://www.graphpad.com/
R v3.6.3	R Core Team, 2020	https://cran.r-project.org/
StepOne software v2.3	Thermo Fisher Scientific	https://www.thermofisher.com/

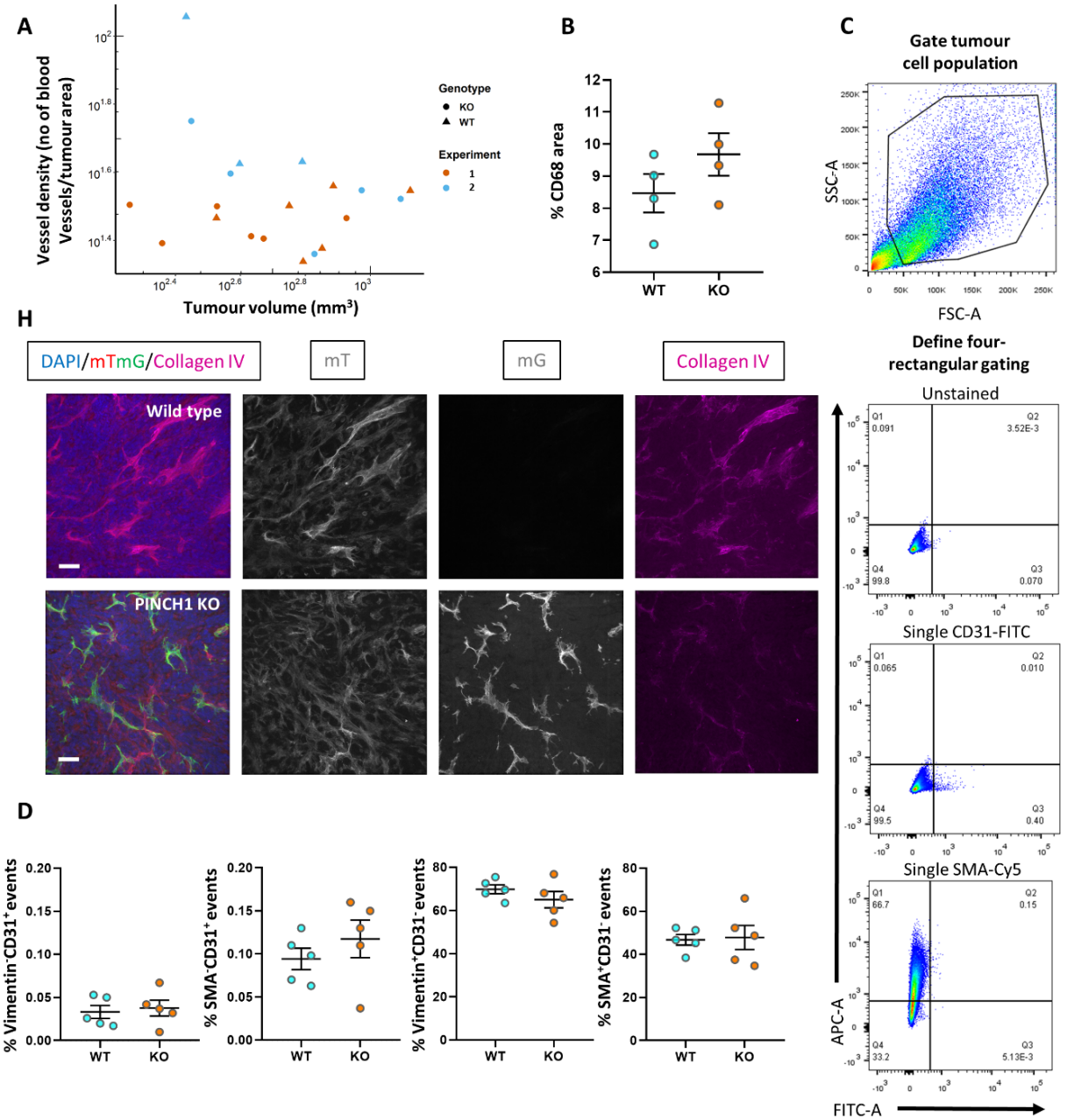
A
Vessel density (no of blood Vessels/tumour area)
Tumour volume (mm³)
Genotype
KO
WT
Experiment
1
2
B
% CD68 area
WT
KO
C
Gate tumour cell population
SSC-A
FSC-A
H
DAPI/mTmG/Collagen IV
mT
mG
Collagen IV
Wild type
PINCH1 KO
Define four-rectangular gating
Unstained
Single CD31-FITC
Single SMA-Cy5
APC-A
FITC-A
D
% Vimentin⁻CD31⁺events
% SMA⁻CD31⁺events
% Vimentin⁺CD31⁻events
% SMA⁺CD31⁻events
E
Vimentin
aSMA
Events
APC-A
F
% Vimentin⁺events
% SMA⁺events
G
MFI Vimentin
MFI SMA

Supplementary Figure. Investigating the impact of EC PINCH1 deletion in TME components of CMT19 tumour models. (A) Scatter plot showing the absence of correlation between B16F0 tumour volume and vessel density. **(B)** Percentages of $CD68^+$ area per tile scanned section from CMT19 tumours (One experiment; Wild type, N=4; KO, N=4). **(C)** Gating strategy: The tumour cell population is gated from the total events collected. Then, the four-rectangular gating is defined on the unstained sample and applied in all stained samples to distinguish double negative, single positive and double positive events. **(D)** Percentages of $vimentin^+CD31^-$, $aSMA^+CD31^-$, $vimentin^-CD31^+$ and $aSMA^-CD31^+$ events from CMT19 tumour-bearing control and KO mice. **(E)** Histograms for total number of $aSMA^+$ and $vimentin^+$ events (y axis) over intensity of expression (x axis) in wild type (cyan) and KO (orange) tumours. The unstained control sample is shown in grey. **(F)** Percentages of total $aSMA^+$ and $vimentin^+$ events from CMT19 tumour-bearing control and KO mice. **(G)** Mean fluorescence intensity of total $aSMA^+$ and $vimentin^+$ events. FACS data derive from one experiment. **(H)** Immunofluorescence staining of thick tumour sections for collagen IV (magenta). On merged images, mTmG signal is shown in red (mT) and green (mG). Single mT and mG images for vessel visualization are shown in grey. Cell nuclei were labelled with DAPI (blue). Images were acquired using confocal microscopy (Two experiments: Wild type, N=3; KO, N=4); Objective 25×; Scale bar 50 um. Dot plots were constructed using GraphPad Prism 8.

6. REFERENCES

1. Hanahan, D. & Weinberg, R. A. The Hallmarks of Cancer. *Cell* **100**, 57–70 (2000).
2. Hanahan, D. & Weinberg, R. A. Hallmarks of cancer: the next generation. *Cell* **144**, 646–674 (2011).
3. Wu, T. & Dai, Y. Tumor microenvironment and therapeutic response. *Cancer Lett.* **387**, 61–68 (2017).
4. Balkwill, F. R., Capasso, M. & Hagemann, T. The tumor microenvironment at a glance. *J Cell Sci* **125**, 5591–5596 (2012).
5. Salmon, H., Remark, R., Gnjatic, S. & Merad, M. Host tissue determinants of tumour immunity. *Nature Reviews Cancer* **19**, 215–227 (2019).
6. Turley, S. J., Cremasco, V. & Astarita, J. L. Immunological hallmarks of stromal cells in the tumour microenvironment. *Nat. Rev. Immunol.* **15**, 669–682 (2015).
7. Baghban, R. *et al.* Tumor microenvironment complexity and therapeutic implications at a glance. *Cell Communication and Signaling* **18**, 59 (2020).
8. Carmeliet, P. & Jain, R. K. Molecular mechanisms and clinical applications of angiogenesis. *Nature* **473**, 298–307 (2011).
9. Meacham, C. E. & Morrison, S. J. Tumor heterogeneity and cancer cell plasticity. *Nature* **501**, 328–337 (2013).
10. Adams, R. H. & Alitalo, K. Molecular regulation of angiogenesis and lymphangiogenesis. *Nat. Rev. Mol. Cell Biol.* **8**, 464–478 (2007).
11. *Fundamentals of Vascular Biology*. (Springer International Publishing, 2019). doi:10.1007/978-3-030-12270-6.
12. Jain, R. K. Molecular regulation of vessel maturation. *Nat. Med.* **9**, 685–693 (2003).
13. Kolte, D., McClung, J. A. & Aronow, W. S. Chapter 6 - Vasculogenesis and Angiogenesis. in *Translational Research in Coronary Artery Disease* (eds. Aronow, W. S. & McClung, J. A.) 49–65 (Academic Press, 2016). doi:10.1016/B978-0-12-802385-3.00006-1.
14. Garcia, M. D. & Larina, I. V. Vascular development and hemodynamic force in the mouse yolk sac. *Front. Physiol.* **5**, (2014).
15. Lamalice, L., Le Boeuf, F. & Huot, J. Endothelial cell migration during angiogenesis. *Circ. Res.* **100**, 782–794 (2007).
16. Fong, G. H., Rossant, J., Gertsenstein, M. & Breitman, M. L. Role of the Flt-1 receptor tyrosine kinase in regulating the assembly of vascular endothelium. *Nature* **376**, 66–70 (1995).
17. Shalaby, F. *et al.* Failure of blood-island formation and vasculogenesis in Flk-1-deficient mice. *Nature* **376**, 62–66 (1995).
18. Agah Ramtin *et al.* Cardiovascular Overexpression of Transforming Growth Factor-β1 Causes Abnormal Yolk Sac Vasculogenesis and Early Embryonic Death. *Circulation Research* **86**, 1024–1030 (2000).

19. Dyer, M. A., Farrington, S. M., Mohn, D., Munday, J. R. & Baron, M. H. Indian hedgehog activates hematopoiesis and vasculogenesis and can respecify prospective neurectodermal cell fate in the mouse embryo. *Development* **128**, 1717–1730 (2001).
20. Risau, W. & Flamme, I. Vasculogenesis. *Annual Review of Cell and Developmental Biology* **11**, 73–91 (1995).
21. Asahara, T. *et al.* Bone marrow origin of endothelial progenitor cells responsible for postnatal vasculogenesis in physiological and pathological neovascularization. *Circ. Res.* **85**, 221–228 (1999).
22. Herbert, S. P. & Stainier, D. Y. R. Molecular control of endothelial cell behaviour during blood vessel morphogenesis. *Nat. Rev. Mol. Cell Biol.* **12**, 551–564 (2011).
23. Belle, J. *et al.* Stretch-induced intussuceptive and sprouting angiogenesis in the chick chorioallantoic membrane. *Microvascular Research* **95**, 60–67 (2014).
24. Lee, G. S. *et al.* Blood flow shapes intravascular pillar geometry in the chick chorioallantoic membrane. *J Angiogenes Res* **2**, 11 (2010).
25. Filipovic, N. *et al.* Computational flow dynamics in a geometric model of intussusceptive angiogenesis. *Microvasc. Res.* **78**, 286–293 (2009).
26. Baum, O. *et al.* VEGF-A Promotes Intussusceptive Angiogenesis in the Developing Chicken Chorioallantoic Membrane. *Microcirculation* **17**, 447–457 (2010).
27. Gianni-Barrera, R., Bartolomeo, M., Vollmar, B., Djonov, V. & Banfi, A. Split for the cure: VEGF, PDGF-BB and intussusception in therapeutic angiogenesis. *Biochem. Soc. Trans.* **42**, 1637–1642 (2014).
28. Betz, C., Lenard, A., Belting, H.-G. & Affolter, M. Cell behaviors and dynamics during angiogenesis. *Development* **143**, 2249–2260 (2016).
29. Blanco, R. & Gerhardt, H. VEGF and Notch in tip and stalk cell selection. *Cold Spring Harb Perspect Med* **3**, a006569 (2013).
30. Germain, S., Monnot, C., Muller, L. & Eichmann, A. Hypoxia-driven angiogenesis: role of tip cells and extracellular matrix scaffolding. *Curr. Opin. Hematol.* **17**, 245–251 (2010).
31. Gerhardt, H. *et al.* VEGF guides angiogenic sprouting utilizing endothelial tip cell filopodia. *J. Cell Biol.* **161**, 1163–1177 (2003).
32. Potente, M., Gerhardt, H. & Carmeliet, P. Basic and therapeutic aspects of angiogenesis. *Cell* **146**, 873–887 (2011).
33. Augustin, H. G., Koh, G. Y., Thurston, G. & Alitalo, K. Control of vascular morphogenesis and homeostasis through the angiopoietin-Tie system. *Nat. Rev. Mol. Cell Biol.* **10**, 165–177 (2009).
34. Geudens, I. & Gerhardt, H. Coordinating cell behaviour during blood vessel formation. *Development* **138**, 4569–4583 (2011).
35. Phng, L.-K. & Gerhardt, H. Angiogenesis: a team effort coordinated by notch. *Dev. Cell* **16**, 196–208 (2009).

36. Jakobsson, L. *et al.* Endothelial cells dynamically compete for the tip cell position during angiogenic sprouting. *Nat. Cell Biol.* **12**, 943–953 (2010).
37. Arima, S. *et al.* Angiogenic morphogenesis driven by dynamic and heterogeneous collective endothelial cell movement. *Development* **138**, 4763–4776 (2011).
38. Siekmann, A. F., Affolter, M. & Belting, H.-G. The tip cell concept 10 years after: new players tune in for a common theme. *Exp. Cell Res.* **319**, 1255–1263 (2013).
39. Pontes-Quero, S. *et al.* High mitogenic stimulation arrests angiogenesis. *Nature Communications* **10**, 1–16 (2019).
40. Costa, G. *et al.* Asymmetric division coordinates collective cell migration in angiogenesis. *Nat. Cell Biol.* **18**, 1292–1301 (2016).
41. Adams, R. H. & Eichmann, A. Axon Guidance Molecules in Vascular Patterning. *Cold Spring Harb Perspect Biol* **2**, (2010).
42. Carmeliet, P. & Tessier-Lavigne, M. Common mechanisms of nerve and blood vessel wiring. *Nature* **436**, 193–200 (2005).
43. Zeng, G. *et al.* Orientation of endothelial cell division is regulated by VEGF signaling during blood vessel formation. *Blood* **109**, 1345–1352 (2007).
44. Phng, L.-K. *et al.* Nrarp coordinates endothelial Notch and Wnt signaling to control vessel density in angiogenesis. *Dev. Cell* **16**, 70–82 (2009).
45. Charpentier, M. S. & Conlon, F. L. Cellular and molecular mechanisms underlying blood vessel lumen formation. *BioEssays* **36**, 251–259 (2014).
46. Blum, Y. *et al.* Complex cell rearrangements during intersegmental vessel sprouting and vessel fusion in the zebrafish embryo. *Dev. Biol.* **316**, 312–322 (2008).
47. Fantin, A. *et al.* Tissue macrophages act as cellular chaperones for vascular anastomosis downstream of VEGF-mediated endothelial tip cell induction. *Blood* **116**, 829–840 (2010).
48. Pardali, E., Goumans, M.-J. & ten Dijke, P. Signaling by members of the TGF-beta family in vascular morphogenesis and disease. *Trends Cell Biol.* **20**, 556–567 (2010).
49. Gaengel, K., Genové, G., Armulik, A. & Betsholtz, C. Endothelial-mural cell signaling in vascular development and angiogenesis. *Arterioscler. Thromb. Vasc. Biol.* **29**, 630–638 (2009).
50. Franco, C. A. *et al.* Dynamic Endothelial Cell Rearrangements Drive Developmental Vessel Regression. *PLOS Biology* **13**, e1002125 (2015).
51. Chung, A. S., Lee, J. & Ferrara, N. Targeting the tumour vasculature: insights from physiological angiogenesis. *Nat. Rev. Cancer* **10**, 505–514 (2010).
52. Nico, B. *et al.* Intussusceptive microvascular growth in human glioma. *Clin. Exp. Med.* **10**, 93–98 (2010).
53. Patan, S., Munn, L. L. & Jain, R. K. Intussusceptive microvascular growth in a human colon adenocarcinoma xenograft: a novel mechanism of tumor angiogenesis. *Microvasc. Res.* **51**, 260–272 (1996).

54. Ribatti, D. *et al.* Microvascular density, vascular endothelial growth factor immunoreactivity in tumor cells, vessel diameter and intussusceptive microvascular growth in primary melanoma. *Oncol. Rep.* **14**, 81–84 (2005).
55. Lyden, D. *et al.* Impaired recruitment of bone-marrow-derived endothelial and hematopoietic precursor cells blocks tumor angiogenesis and growth. *Nat. Med.* **7**, 1194–1201 (2001).
56. Zuazo-Gaztelu, I. & Casanovas, O. Unraveling the Role of Angiogenesis in Cancer Ecosystems. *Front Oncol* **8**, 248 (2018).
57. Hendrix, M. J. C., Seftor, E. A., Hess, A. R. & Seftor, R. E. B. Vasculogenic mimicry and tumour-cell plasticity: lessons from melanoma. *Nat. Rev. Cancer* **3**, 411–421 (2003).
58. Cheng, L. *et al.* Glioblastoma stem cells generate vascular pericytes to support vessel function and tumor growth. *Cell* **153**, 139–152 (2013).
59. Ricci-Vitiani, L. *et al.* Tumour vascularization via endothelial differentiation of glioblastoma stem-like cells. *Nature* **468**, 824–828 (2010).
60. Wang, R. *et al.* Glioblastoma stem-like cells give rise to tumour endothelium. *Nature* **468**, 829–833 (2010).
61. Bergers, G. & Benjamin, L. E. Tumorigenesis and the angiogenic switch. *Nat. Rev. Cancer* **3**, 401–410 (2003).
62. Kuczynski, E. A., Vermeulen, P. B., Pezzella, F., Kerbel, R. S. & Reynolds, A. R. Vessel co-option in cancer. *Nature Reviews Clinical Oncology* **16**, 469–493 (2019).
63. Lugano, R., Ramachandran, M. & Dimberg, A. Tumor angiogenesis: causes, consequences, challenges and opportunities. *Cell. Mol. Life Sci.* (2019) doi:10.1007/s00018-019-03351-7.
64. Jain, R. K. Normalization of tumor vasculature: an emerging concept in antiangiogenic therapy. *Science* **307**, 58–62 (2005).
65. Nagy, J. A., Chang, S.-H., Dvorak, A. M. & Dvorak, H. F. Why are tumour blood vessels abnormal and why is it important to know? *Br. J. Cancer* **100**, 865–869 (2009).
66. Dewhirst, M. W. & Secomb, T. W. Transport of drugs from blood vessels to tumour tissue. *Nature Reviews Cancer* **17**, 738–750 (2017).
67. Schaaf, M. B., Garg, A. D. & Agostinis, P. Defining the role of the tumor vasculature in antitumor immunity and immunotherapy. *Cell Death & Disease* **9**, 1–14 (2018).
68. Hendry, S. A. *et al.* The Role of the Tumor Vasculature in the Host Immune Response: Implications for Therapeutic Strategies Targeting the Tumor Microenvironment. *Front Immunol* **7**, (2016).
69. Dudley, A. C. Tumor Endothelial Cells. *Cold Spring Harb Perspect Med* **2**, (2012).
70. De Palma, M., Biziato, D. & Petrova, T. V. Microenvironmental regulation of tumour angiogenesis. *Nat. Rev. Cancer* **17**, 457–474 (2017).
71. Ribatti, D., Nico, B., Crivellato, E. & Vacca, A. The structure of the vascular network of tumors. *Cancer Lett.* **248**, 18–23 (2007).

72. Potente, M. & Carmeliet, P. The Link Between Angiogenesis and Endothelial Metabolism. *Annual Review of Physiology* **79**, 43–66 (2017).
73. Hida, K., Maishi, N., Annan, D. A. & Hida, Y. Contribution of Tumor Endothelial Cells in Cancer Progression. *Int J Mol Sci* **19**, (2018).
74. Armulik, A., Genové, G. & Betsholtz, C. Pericytes: developmental, physiological, and pathological perspectives, problems, and promises. *Dev. Cell* **21**, 193–215 (2011).
75. Vasudev, N. S. & Reynolds, A. R. Anti-angiogenic therapy for cancer: current progress, unresolved questions and future directions. *Angiogenesis* **17**, 471–494 (2014).
76. Matsumoto, K. & Ema, M. Roles of VEGF-A signalling in development, regeneration, and tumours. *J. Biochem.* **156**, 1–10 (2014).
77. Holmes, D. I. & Zachary, I. The vascular endothelial growth factor (VEGF) family: angiogenic factors in health and disease. *Genome Biol* **6**, 209 (2005).
78. Carmeliet, P. VEGF as a key mediator of angiogenesis in cancer. *Oncology* **69 Suppl 3**, 4–10 (2005).
79. Ferrara, N. *et al.* Heterozygous embryonic lethality induced by targeted inactivation of the VEGF gene. *Nature* **380**, 439–442 (1996).
80. Carmeliet, P. *et al.* Abnormal blood vessel development and lethality in embryos lacking a single VEGF allele. *Nature* **380**, 435–439 (1996).
81. Miquerol, L., Langille, B. L. & Nagy, A. Embryonic development is disrupted by modest increases in vascular endothelial growth factor gene expression. *Development* **127**, 3941–3946 (2000).
82. Wong, P.-P., Bodrug, N. & Hodivala-Dilke, K. M. Exploring Novel Methods for Modulating Tumor Blood Vessels in Cancer Treatment. *Current Biology* **26**, R1161–R1166 (2016).
83. Mancuso, M. R. *et al.* Rapid vascular regrowth in tumors after reversal of VEGF inhibition. *J. Clin. Invest.* **116**, 2610–2621 (2006).
84. Kerbel, R. S. Tumor angiogenesis. *N. Engl. J. Med.* **358**, 2039–2049 (2008).
85. Elice, F. & Rodeghiero, F. Side effects of anti-angiogenic drugs. *Thromb. Res.* **129 Suppl 1**, S50-53 (2012).
86. Winkler, F. *et al.* Kinetics of vascular normalization by VEGFR2 blockade governs brain tumor response to radiation: role of oxygenation, angiopoietin-1, and matrix metalloproteinases. *Cancer Cell* **6**, 553–563 (2004).
87. Jain, R. K., Duda, D. G., Clark, J. W. & Loeffler, J. S. Lessons from phase III clinical trials on anti-VEGF therapy for cancer. *Nat Clin Pract Oncol* **3**, 24–40 (2006).
88. Wong, P.-P. *et al.* Dual-action combination therapy enhances angiogenesis while reducing tumor growth and spread. *Cancer Cell* **27**, 123–137 (2015).
89. Saman, H., Raza, S. S., Uddin, S. & Rasul, K. Inducing Angiogenesis, a Key Step in Cancer Vascularization, and Treatment Approaches. *Cancers (Basel)* **12**, (2020).

90. Bridges, E. & Harris, A. L. Vascular-promoting therapy reduced tumor growth and progression by improving chemotherapy efficacy. *Cancer Cell* **27**, 7–9 (2015).
91. Hynes, R. O. Integrins: Bidirectional, Allosteric Signaling Machines. *Cell* **110**, 673–687 (2002).
92. Humphries, J. D., Byron, A. & Humphries, M. J. Integrin ligands at a glance. *Journal of Cell Science* **119**, 3901–3903 (2006).
93. Hamidi, H. & Ivaska, J. Every step of the way: integrins in cancer progression and metastasis. *Nature Reviews Cancer* **18**, 533–548 (2018).
94. Harburger, D. S. & Calderwood, D. A. Integrin signalling at a glance. *Journal of Cell Science* **122**, 159–163 (2009).
95. Seguin, L., Desgrosellier, J. S., Weis, S. M. & Cheresh, D. A. Integrins and cancer: regulators of cancer stemness, metastasis, and drug resistance. *Trends Cell Biol* **25**, 234–240 (2015).
96. Desgrosellier, J. S. & Cheresh, D. A. Integrins in cancer: biological implications and therapeutic opportunities. *Nat. Rev. Cancer* **10**, 9–22 (2010).
97. Cooper, J. & Giancotti, F. G. Integrin Signaling in Cancer: Mechanotransduction, Stemness, Epithelial Plasticity, and Therapeutic Resistance. *Cancer Cell* **35**, 347–367 (2019).
98. Weis, S. M. & Cheresh, D. A. αv Integrins in Angiogenesis and Cancer. *Cold Spring Harb Perspect Med* **1**, (2011).
99. Robinson, S. D. & Hodivala-Dilke, K. M. The role of β3-integrins in tumor angiogenesis: context is everything. *Curr. Opin. Cell Biol.* **23**, 630–637 (2011).
100. Avraamides, C. J., Garmy-Susini, B. & Varner, J. A. Integrins in angiogenesis and lymphangiogenesis. *Nat Rev Cancer* **8**, 604–617 (2008).
101. Li, H. *et al.* Structural basis of kindlin-mediated integrin recognition and activation. *Proc. Natl. Acad. Sci. U.S.A.* **114**, 9349–9354 (2017).
102. Klapholz, B. & Brown, N. H. Talin – the master of integrin adhesions. *J Cell Sci* **130**, 2435–2446 (2017).
103. Franceschi, N. D., Hamidi, H., Alanko, J., Sahgal, P. & Ivaska, J. Integrin traffic – the update. *J Cell Sci* **128**, 839–852 (2015).
104. Nader, G. P. F., Ezratty, E. J. & Gundersen, G. G. FAK, talin and PIPKIγ regulate endocytosed integrin activation to polarize focal adhesion assembly. *Nat. Cell Biol.* **18**, 491–503 (2016).
105. Barrow-McGee, R. *et al.* Beta 1-integrin–c-Met cooperation reveals an inside-in survival signalling on autophagy-related endomembranes. *Nature Communications* **7**, 11942 (2016).
106. Alanko, J. *et al.* Integrin endosomal signalling suppresses anoikis. *Nat Cell Biol* **17**, 1412–1421 (2015).
107. Michael, M. & Parsons, M. New perspectives on integrin-dependent adhesions. *Current Opinion in Cell Biology* **63**, 31–37 (2020).
108. Winograd-Katz, S. E., Fässler, R., Geiger, B. & Legate, K. R. The integrin adhesome: from genes and proteins to human disease. *Nat. Rev. Mol. Cell Biol.* **15**, 273–288 (2014).

109. Geiger, B. & Yamada, K. M. Molecular architecture and function of matrix adhesions. *Cold Spring Harb Perspect Biol* **3**, (2011).

110. Geiger, B., Spatz, J. P. & Bershadsky, A. D. Environmental sensing through focal adhesions. *Nat. Rev. Mol. Cell Biol.* **10**, 21–33 (2009).

111. Byron, A., Morgan, M. R. & Humphries, M. J. Adhesion signalling complexes. *Curr Biol* **20**, R1063–R1067 (2010).

112. Linder, S. & Kopp, P. Podosomes at a glance. *Journal of Cell Science* **118**, 2079–2082 (2005).

113. Zaidel-Bar, R., Itzkovitz, S., Ma'ayan, A., Iyengar, R. & Geiger, B. Functional atlas of the integrin adhesome. *Nature Cell Biology* **9**, 858–867 (2007).

114. Zaidel-Bar, R. & Geiger, B. The switchable integrin adhesome. *J. Cell. Sci.* **123**, 1385–1388 (2010).

115. Horton, E. R. *et al.* Definition of a consensus integrin adhesome and its dynamics during adhesion complex assembly and disassembly. *Nature Cell Biology* **17**, 1577–1587 (2015).

116. Kanchanawong, P. *et al.* Nanoscale architecture of integrin-based cell adhesions. *Nature* **468**, 580–584 (2010).

117. Horton, E. R. *et al.* The integrin adhesome network at a glance. *J Cell Sci* **129**, 4159–4163 (2016).

118. Humphries, J. D., Chastney, M. R., Askari, J. A. & Humphries, M. J. Signal transduction via integrin adhesion complexes. *Curr. Opin. Cell Biol.* **56**, 14–21 (2019).

119. Horton, E. R., Astudillo, P., Humphries, M. J. & Humphries, J. D. Mechanosensitivity of integrin adhesion complexes: role of the consensus adhesome. *Exp. Cell Res.* **343**, 7–13 (2016).

120. Kadrmas, J. L. & Beckerle, M. C. The LIM domain: from the cytoskeleton to the nucleus. *Nat. Rev. Mol. Cell Biol.* **5**, 920–931 (2004).

121. Wu, C. The PINCH–ILK–parvin complexes: assembly, functions and regulation. *Biochimica et Biophysica Acta (BBA) - Molecular Cell Research* **1692**, 55–62 (2004).

122. Ghatak, S., Morgner, J. & Wickström, S. A. ILK: a pseudokinase with a unique function in the integrin-actin linkage. *Biochem. Soc. Trans.* **41**, 995–1001 (2013).

123. Wu, C. The PINCH–ILK–parvin complexes: assembly, functions and regulation. *Biochimica et Biophysica Acta (BBA) - Molecular Cell Research* **1692**, 55–62 (2004).

124. Wu, C. PINCH, N(i)ck and the ILK: network wiring at cell-matrix adhesions. *Trends Cell Biol.* **15**, 460–466 (2005).

125. Legate, K. R., Montañez, E., Kudlacek, O. & Fässler, R. ILK, PINCH and parvin: the tIPP of integrin signalling. *Nat. Rev. Mol. Cell Biol.* **7**, 20–31 (2006).

126. Wickström, S. A., Lange, A., Montanez, E. & Fässler, R. The ILK/PINCH/parvin complex: the kinase is dead, long live the pseudokinase! *EMBO J.* **29**, 281–291 (2010).

127. Dougherty, G. W., Chopp, T., Qi, S. & Cutler, M. L. The Ras suppressor Rsu-1 binds to the LIM 5 domain of the adaptor protein PINCH1 and participates in adhesion-related functions. *Experimental Cell Research* **306**, 168–179 (2005).

128. Sakai, T. *et al.* Integrin-linked kinase (ILK) is required for polarizing the epiblast, cell adhesion, and controlling actin accumulation. *Genes Dev.* **17**, 926–940 (2003).

129. Liang, X. *et al.* PINCH1 Plays an Essential Role in Early Murine Embryonic Development but Is Dispensable in Ventricular Cardiomyocytes. *Mol Cell Biol* **25**, 3056–3062 (2005).

130. Montanez, E., Wickström, S. A., Altstätter, J., Chu, H. & Fässler, R. α-parvin controls vascular mural cell recruitment to vessel wall by regulating RhoA/ROCK signalling. *EMBO J* **28**, 3132–3144 (2009).

131. Chu, H. *et al.* γ-Parvin Is Dispensable for Hematopoiesis, Leukocyte Trafficking, and T-Cell-Dependent Antibody Response. *Mol Cell Biol* **26**, 1817–1825 (2006).

132. Stanchi, F. *et al.* Consequences of loss of PINCH2 expression in mice. *Journal of Cell Science* **118**, 5899–5910 (2005).

133. Braun, A. *et al.* PINCH2 is a new five LIM domain protein, homologous to PINCHand localized to focal adhesions☆. *Experimental Cell Research* **284**, 237–248 (2003).

134. Korenbaum, E., Olski, T. M. & Noegel, A. A. Genomic organization and expression profile of the parvin family of focal adhesion proteins in mice and humans. *Gene* **279**, 69–79 (2001).

135. Fukuda, T., Chen, K., Shi, X. & Wu, C. PINCH-1 is an obligate partner of integrin-linked kinase (ILK) functioning in cell shape modulation, motility, and survival. *J. Biol. Chem.* **278**, 51324–51333 (2003).

136. Zhang, Y., Chen, K., Tu, Y. & Wu, C. Distinct Roles of Two Structurally Closely Related Focal Adhesion Proteins, α-Parvins and β-Parvins, in Regulation of Cell Morphology and Survival. *J. Biol. Chem.* **279**, 41695–41705 (2004).

137. Legate, K. R., Montañez, E., Kudlacek, O. & Fässler, R. ILK, PINCH and parvin: the tIPP of integrin signalling. *Nat. Rev. Mol. Cell Biol.* **7**, 20–31 (2006).

138. Clark, K. A., McGrail, M. & Beckerle, M. C. Analysis of PINCH function in Drosophila demonstrates its requirement in integrin-dependent cellular processes. *Development* **130**, 2611–2621 (2003).

139. Hobert, O., Moerman, D. G., Clark, K. A., Beckerle, M. C. & Ruvkun, G. A conserved LIM protein that affects muscular adherens junction integrity and mechanosensory function in Caenorhabditis elegans. *J. Cell Biol.* **144**, 45–57 (1999).

140. Li, S. *et al.* PINCH1 regulates cell-matrix and cell-cell adhesions, cell polarity and cell survival during the peri-implantation stage. *J. Cell. Sci.* **118**, 2913–2921 (2005).

141. Karaköse, E. *et al.* The focal adhesion protein PINCH-1 associates with EPLIN at integrin adhesion sites. *J Cell Sci* **128**, 1023–1033 (2015).

142. Liang, X. *et al.* Targeted ablation of PINCH1 and PINCH2 from murine myocardium results in dilated cardiomyopathy and early postnatal lethality. *Circulation* **120**, 568–576 (2009).

143. Wang, Y. *et al.* Focal adhesion proteins Pinch1 and Pinch2 regulate bone homeostasis in mice. *JCI Insight* **4**, (2019).

144. Donthamsetty, S. *et al.* Role of PINCH and Its Partner Tumor Suppressor Rsu-1 in Regulating Liver Size and Tumorigenesis. *PLOS ONE* **8**, e74625 (2013).

145. Kogata, N., Tribe, R. M., Fässler, R., Way, M. & Adams, R. H. Integrin-linked kinase controls vascular wall formation by negatively regulating Rho/ROCK-mediated vascular smooth muscle cell contraction. *Genes Dev* **23**, 2278–2283 (2009).

146. Park, H. *et al.* Integrin-linked kinase controls retinal angiogenesis and is linked to Wnt signaling and exudative vitreoretinopathy. *Nature Communications* **10**, 5243 (2019).

147. Friedrich, E. B. *et al.* Integrin-linked kinase regulates endothelial cell survival and vascular development. *Mol. Cell. Biol.* **24**, 8134–8144 (2004).

148. Fraccaroli, A. *et al.* Endothelial alpha-parvin controls integrity of developing vasculature and is required for maintenance of cell-cell junctions. *Circ. Res.* **117**, 29–40 (2015).

149. Xu, H., Cao, H. & Xiao, G. Signaling via PINCH: Functions, binding partners and implications in human diseases. *Gene* **594**, 10–15 (2016).

150. Cabodi, S., del Pilar Camacho-Leal, M., Di Stefano, P. & Defilippi, P. Integrin signalling adaptors: not only figurants in the cancer story. *Nature Reviews Cancer* **10**, 858–870 (2010).

151. Wang-Rodriguez, J., Dreilinger, A. D., Alsharabi, G. M. & Rearden, A. The signaling adapter protein PINCH is up-regulated in the stroma of common cancers, notably at invasive edges. *Cancer* **95**, 1387–1395 (2002).

152. Gao, J., Arbman, G., Rearden, A. & Sun, X.-F. Stromal Staining for PINCH Is an Independent Prognostic Indicator in Colorectal Cancer. *Neoplasia* **6**, 796–801 (2004).

153. Wang, M.-W. *et al.* Expression of PINCH protein in gliomas and its clinicopathological significance. *Oncology* **72**, 343–346 (2007).

154. Kovalevich, J., Tracy, B. & Langford, D. PINCH: More than just an adaptor protein in cellular response. *J. Cell. Physiol.* **226**, 940–947 (2011).

155. Zhang, J.-T. *et al.* Up-regulation of PINCH in the stroma of oral squamous cell carcinoma predicts nodal metastasis. *Oncol. Rep.* **14**, 1519–1522 (2005).

156. Zhu, Z.-L. *et al.* PINCH expression and its clinicopathological significance in gastric adenocarcinoma. *Dis. Markers* **33**, 171–178 (2012).

157. Claxton, S. *et al.* Efficient, inducible Cre-recombinase activation in vascular endothelium. *Genesis* **46**, 74–80 (2008).

158. Reynolds, L. E. & Hodivala-Dilke, K. M. Primary mouse endothelial cell culture for assays of angiogenesis. *Methods Mol. Med.* **120**, 503–509 (2006).

159. R Core Team (2020). R: A language and environment for statistical computing. R Foundation for Statistical Computing, Vienna, Austria.

160. Wickham, H. *ggplot2: Elegant Graphics for Data Analysis*. (Springer-Verlag, 2009). doi:10.1007/978-0-387-98141-3.

161. Seynhaeve, A. L. B. *et al.* Spatiotemporal endothelial cell – pericyte association in tumors as shown by high resolution 4D intravital imaging. *Scientific Reports* **8**, 9596 (2018).

162. Snyder, C. S. *et al.* A dual-color genetically engineered mouse model for multispectral imaging of the pancreatic microenvironment. *Pancreas* **42**, 952–958 (2013).

163. Seynhaeve, A. L. B. & Hagen, T. L. M. ten. Intravital Microscopy of Tumor-associated Vasculature Using Advanced Dorsal Skinfold Window Chambers on Transgenic Fluorescent Mice. *JoVE (Journal of Visualized Experiments)* e55115 (2018) doi:10.3791/55115.

164. Chen, X., Nadiarynkh, O., Plotnikov, S. & Campagnola, P. J. Second harmonic generation microscopy for quantitative analysis of collagen fibrillar structure. *Nat Protoc* **7**, 654–669 (2012).

165. Lattouf, R. *et al.* Picrosirius red staining: a useful tool to appraise collagen networks in normal and pathological tissues. *J. Histochem. Cytochem.* **62**, 751–758 (2014).

166. Ciszewski, W. M. *et al.* The ILK-MMP9-MRTF axis is crucial for EndMT differentiation of endothelial cells in a tumor microenvironment. *Biochimica et Biophysica Acta (BBA) - Molecular Cell Research* **1864**, 2283–2296 (2017).

167. Hortelano, S. *et al.* ILK mediates LPS-induced vascular adhesion receptor expression and subsequent leucocyte trans-endothelial migration. *Cardiovasc Res* **86**, 283–292 (2010).

168. Vouret-Craviari, V., Boulter, E., Grall, D., Matthews, C. & Obberghen-Schilling, E. V. ILK is required for the assembly of matrix-forming adhesions and capillary morphogenesis in endothelial cells. *Journal of Cell Science* **117**, 4559–4569 (2004).

169. Malan, D. *et al.* Deletion of integrin linked kinase in endothelial cells results in defective RTK signaling caused by caveolin 1 mislocalization. *Development* **140**, 987–995 (2013).

170. Edwards, L. A. *et al.* Suppression of VEGF secretion and changes in glioblastoma multiforme microenvironment by inhibition of Integrin-linked kinase (ILK). *Mol Cancer Ther* **7**, 59–70 (2008).

171. Younes, M. N. *et al.* Integrin-linked kinase is a potential therapeutic target for anaplastic thyroid cancer. *Mol Cancer Ther* **4**, 1146–1156 (2005).

172. Tan, C., Mui, A. & Dedhar, S. Integrin-linked Kinase Regulates Inducible Nitric Oxide Synthase and Cyclooxygenase-2 Expression in an NF-κB-dependent Manner. *J. Biol. Chem.* **277**, 3109–3116 (2002).

173. Kaneko, Y., Kitazato, K. & Basaki, Y. Integrin-linked kinase regulates vascular morphogenesis induced by vascular endothelial growth factor. *Journal of Cell Science* **117**, 407–415 (2004).

174. Yau, C. Y. F., Wheeler, J. J., Sutton, K. L. & Hedley, D. W. Inhibition of Integrin-Linked Kinase by a Selective Small Molecule Inhibitor, QLT0254, Inhibits the PI3K/PKB/mTOR, Stat3, and FKHR Pathways and Tumor Growth, and Enhances Gemcitabine-Induced Apoptosis in Human Orthotopic Primary Pancreatic Cancer Xenografts. *Cancer Res* **65**, 1497–1504 (2005).

175. Pitter, B., Werner, A.-C. & Montanez, E. Parvins Are Required for Endothelial Cell-Cell Junctions and Cell Polarity During Embryonic Blood Vessel Formation. *Arterioscler. Thromb. Vasc. Biol.* **38**, 1147–1158 (2018).

176. Tu, Y., Li, F. & Wu, C. Nck-2, a Novel Src Homology2/3-containing Adaptor Protein That Interacts with the LIM-only Protein PINCH and Components of Growth Factor Receptor Kinase-signaling Pathways. *Mol Biol Cell* **9**, 3367–3382 (1998).

177. Li, W., Fan, J. & Woodley, D. T. Nck/Dock: an adapter between cell surface receptors and the actin cytoskeleton. *Oncogene* **20**, 6403–6417 (2001).

178. Zhang, Y., Chen, K., Guo, L. & Wu, C. Characterization of PINCH-2, a New Focal Adhesion Protein That Regulates the PINCH-1-ILK Interaction, Cell Spreading, and Migration. *J. Biol. Chem.* **277**, 38328–38338 (2002).

179. Aguilera, K. Y. & Brekken, R. A. Hypoxia Studies with Pimonidazole in vivo. *Bio Protoc* **4**, (2014).

180. Sei, E. & Conrad, N. K. UV cross-linking of interacting RNA and protein in cultured cells. *Meth. Enzymol.* **539**, 53–66 (2014).

181. Ule, J., Jensen, K., Mele, A. & Darnell, R. B. CLIP: a method for identifying protein-RNA interaction sites in living cells. *Methods* **37**, 376–386 (2005).

182. Kislauskis, E. H., Zhu, X. & Singer, R. H. β-Actin Messenger RNA Localization and Protein Synthesis Augment Cell Motility. *J Cell Biol* **136**, 1263–1270 (1997).

183. Hoog, C. L. de, Foster, L. J. & Mann, M. RNA and RNA Binding Proteins Participate in Early Stages of Cell Spreading through Spreading Initiation Centers. *Cell* **117**, 649–662 (2004).

184. Lee, J. H., Rangarajan, E. S., Yogesha, S. D. & Izard, T. Raver1 interactions with Vinculin and RNA Suggest a Feed-Forward Pathway in Directing mRNA to Focal Adhesions. *Structure* **17**, 833–842 (2009).

185. Babic, I., Sharma, S. & Black, D. L. A Role for Polypyrimidine Tract Binding Protein in the Establishment of Focal Adhesions. *Mol Cell Biol* **29**, 5564–5577 (2009).

186. Willett, M., Pollard, H. J., Vlasak, M. & Morley, S. J. Localization of ribosomes and translation initiation factors to talin/beta3-integrin-enriched adhesion complexes in spreading and migrating mammalian cells. *Biol. Cell* **102**, 265–276 (2010).

187. Atkinson, S. J. *et al.* The β3-integrin endothelial adhesome regulates microtubule-dependent cell migration. *EMBO Rep.* **19**, (2018).

188. Pichon, X., Lagha, M., Mueller, F. & Bertrand, E. A Growing Toolbox to Image Gene Expression in Single Cells: Sensitive Approaches for Demanding Challenges. *Molecular Cell* **71**, 468–480 (2018).